AD-A087 096 UNIVERSITY OF SOUTH FLORIDA TAMPA DEPT OF GEOLOGY F/G 8/3
A DYNAMIC PROCESS MODEL FOR THE BEACH-INLET TRANSITION ZONE.(U)
MAY 80 R A DAVIS, W T FOX N00014-77-C-0151
UNCLASSIFIED TR-3 NL

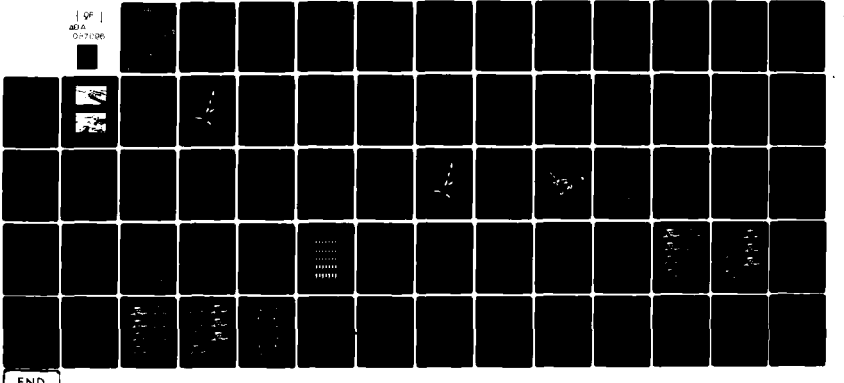

END
DATE FILMED
9-80
DTIC

LEVEL II

12

DEPARTMENT OF GEOLOGY

UNIVERSITY OF SOUTH FLORIDA

Tampa, Florida

33620

12

A DYNAMIC PROCESS MODEL FOR THE BEACH-INLET TRANSITION ZONE

by

Richard A. Davis, Jr., University of South Florida
and
William T. Fox, Williams College

Final Report, May, 1980

of

ONR Task No. 388-136

Contract N00014-77-C-0151

Office of Naval Research

Geography Branch

University of South Florida

Tampa, Florida

This report has been made possible through support and sponsorship by the United States Department of the Navy, Office of Naval Research, under ONR Task Number 388-136, Contract N00014-77-C-0151. Reproduction in whole or in part is permitted for any purpose by the United States Government.

ABSTRACT

Monitoring of tide and wave generated processes and adjacent to Matanzas Inlet, Florida was conducted during the summer of 1978. Data collected include weather parameters, wave and longshore current measurements, tidal currents and morphology of the inlet and adjacent beach and nearshore area. Measurements were made in a time-series mode in order to provide desired input for anticipated modeling of inlet mouth dynamics. Related concurrent projects included drogue studies of tidal currents, sediment transport, bedforms and sediment texture in the inlet.

Weather conditions during the study period were typical of summer conditions on the east coast of Florida. Winds were from the southeast to southwest thereby generating south to north flowing longshore currents. Wind speed was typically less than 10 knots and waves rarely exceeded a meter. Only during the final days of the field study did the wind, wave and longshore current direction shift to a generally north to south direction.

Interactions of tidal inlet processes with open coast processes are significant but restricted to only a few hundred meters of coast adjacent to the inlet. Longshore currents act alternately as a reinforcement and as a hindrance to flow as tides flood and ebb. During flood tides flow on the upcurrent side of the inlet is reinforced and the downcurrent side is hindered. Ebb currents produce the opposite effect on the longshore currents. Beyond the terminal lobe of the ebb tidal delta there is little effect of tidal currents on coastal processes. Here waves are dominant with longshore currents being detectable but masked by waves.

Inlet morphology is an extremely important influence on tidal processes. During flood conditions flow is controlled by channels until shoals are submerged at which time flow is determined primarily by overall inlet shape. Ebbing conditions reflect the reverse situation with channelization of flow during the latter portion of this stage. Numerous locations experience ebb and flood directions which change 30 to 40 degrees as the result of combined effects of sand bodies and channels with the overall shape of the inlet.

The simplistic conditions which prevailed during the study period have permitted construction of a dynamic process model for the beach-inlet transition zone during the tidal cycle. This model depicts the patterns and relative speeds of currents as well as the zones of essentially still water. This model is preliminary and based on only one field study. Further studies and testing of the model are necessary before it can be considered as representative of inlets in general.

TABLE OF CONTENTS

INTRODUCTION

Coastal dynamics include a rather broad variety of wave, current and tide generated processes which operate through a spectrum of environments. The beach and adjacent nearshore zone is a rather uniform environment in terms of coastal processes and their spatial distribution. Process-response studies have resulted in various types of dynamic models for this environment (e.g. Sonu, 1969; Fox and Davis, 1973; 1979).

Inlets have a superficial simplicity dominated by tidal currents which pass over a seemingly uncomplicated substrate. In fact, however, inlets are subjected to wave activity, they have a very complicated detailed morphology and they are influenced to some extent by the processes operating along the open coast. It is this latter question to which the current investigation is addressed. The present research is aimed at trying to establish the nature of the interrelationships between tide-dominated inlet processes and wave dominated open coastal processes. An intense monitoring study of the natural inlet produced the field data from which conceptual and dynamic computer models have been generated. Although the project considers only one inlet, several of the generalizations appear to have widespread application.

Objectives

The overall aim of this project is to conduct a field study that would provide sufficient data for characterizing the existing interrelationships between inlet processes and those which exist on the open marine coast. Using a time-series approach to data collection, the investigators' intent is to provide both a temporal and spatial network of data that will allow construction of various dynamic models of this complicated transition area.

In order to accomplish this task it is necessary to have the array of data collection locations sufficiently extensive so as to include adjacent coastal areas beyond significant inlet influence and also to monitor the inlet itself in order to obtain data unaffected by open coast processes. Variety in coastal conditions is a prerequisite to a comprehensive study of this type and to this end our data are limited. There are no periods of intense storm activity and except for a few days duration, wave and longshore currents are consistently from the south to the north.

Although the investigation is concerned with only one inlet, the broad generalizations realized should have application to other inlets of similar morphology and tidal climate. Further investigations of additional inlets through a broad spectrum of coastal conditions are necessary in order to approach the understanding of inlet-mouth dynamics that will compare with those already achieved for the beach and nearshore zones.

Previous Work

The complex interactions of waves and currents which have application to the open coast-inlet transition zone have been formulated. Longuet-Higgins and Stewart (1960) developed an equation for wave motion which is superimposed on a variable current and they also introduced the concept of radiation stress. Their efforts were expanded by Whitman (1962) who developed the conservation equations for mass, momentum and energy in two dimensions for waves or for varying current. Johnson, Skaugaard and Wang (1971) studied current-depth refraction and solved the transformation of wave length and height for two-dimensional wave interactions. Most of the recent efforts on wave and current interactions are reviewed in Phillips (1966) and Peregrine (1976).

Bruun and Gerritsen (1959) showed the development of ebb and flood channel systems and related sand bodies in the ebb and flood tidal deltas. Detailed morphologic classification of tidal deltas was presented by Hayes, et al (1973) and Hayes (1975). Problems of sediment transport in tidal inlets have been discussed by Bruun (1969) and Ritter (1972). Field study of coastal processes and sediment transport at inlet mouths have been conducted by Finley (1975) at North Inlet and by FitzGerald, et al (1976) at Price Inlet; both in South Carolina. An excellent summary of the state of the art on inlets is provided in a book by Bruun (1968).

General Setting

Matanzas Inlet represents the only unstructured inlet on the east coast of Florida. It is in its natural state except for the highway bridge over its throat (Figure 1) and modest dredging in early 1977. This inlet also functions as the mouth of the Matanzas River which is connected to, or synonomous with, the Intracoastal Waterway at several places. Matanzas Inlet is located in St. Johns County about 20 km south of St. Augustine and 65 km north of Daytona Beach (Figure 1), the sites of the nearest adjacent inlets. The inlet is bounded by Anastasia Island to the north, Summer Haven on the south and Rattlesnake Island on the landward side.

Underlying the unconsolidated sediments in the inlet is the Anastasia Formation of Pleistocene age. This is a unit of variable resistance composed of carbonate cemented biogenic debris (coquina). The Anastasia has some influence on the inlet in that discontinuous exposures crop out just seaward of the highway bridge on the south side of the inlet. During the generally erosional conditions of winter, the Anastasia is well exposed during low tide stage. The inlet contains abundant sand and gravel size sediment which exhibits a distinctly bimodal grain size distribution. The modes consist of sand size quartz and fine gravel shell debris. Although they may be mixed, most of the inlet is dominated by either of the two sediment types (Lee, 1980).

Matanzas Inlet and the surrounding area has been known from historical records which date back to Spanish settlements of the 16th century. Relatively good maps, charts, and aerial photographs are available since 1965 (Mehta and Jones, 1977). Although there have been numerous changes in the inlet during the past two centuries, its overall morphology has

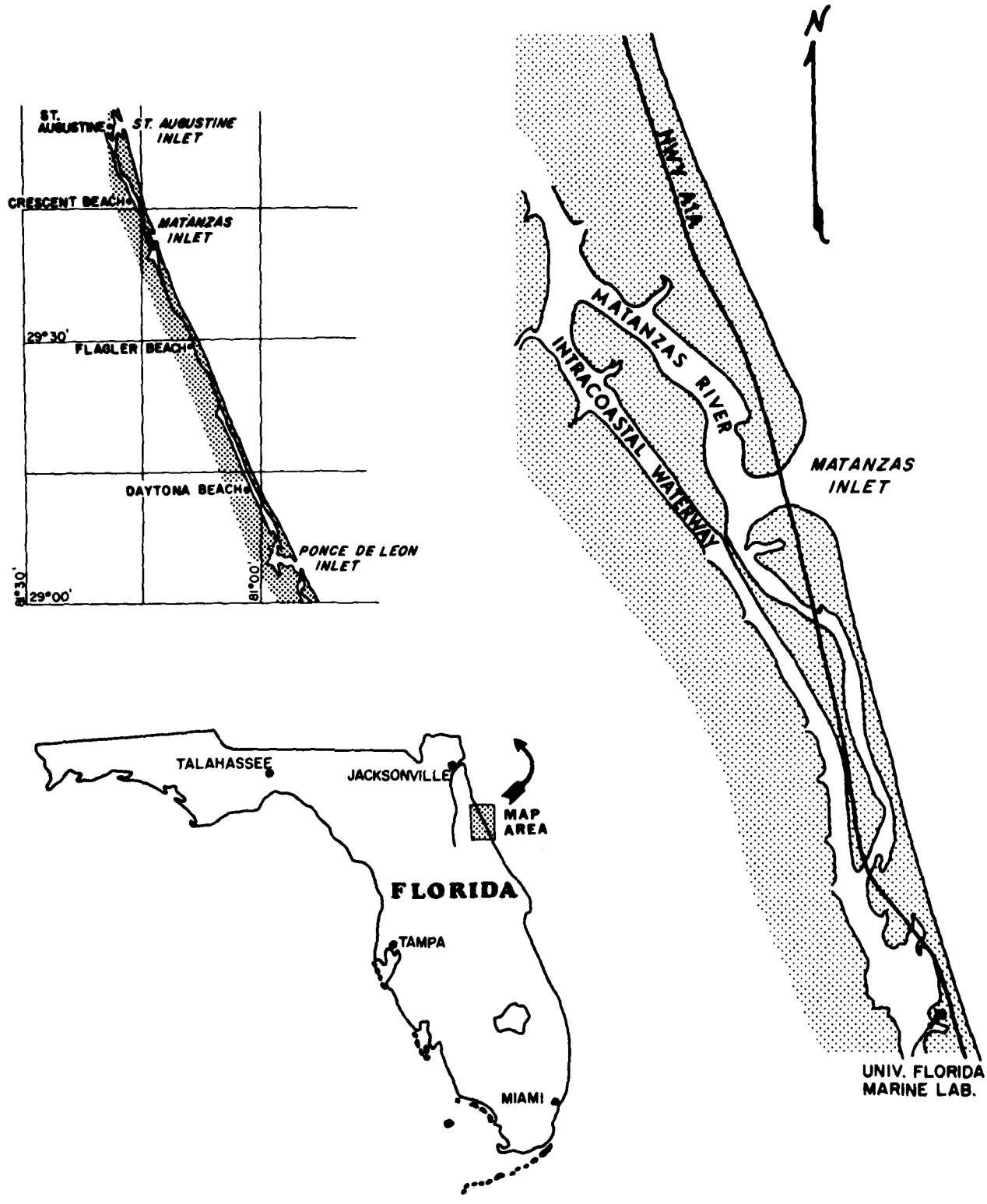

Figure 1. Location map of Matanzas Inlet showing general configuration of the estuary system.

been rather similar. The inlet cross-section has changed but the depth and location of the deep channel have been fairly constant for at least 25 years (Mehta and Jones, 1977). Anastasia Island has shown southerly progradation due to the domination of the south flowing littoral drift system. This trend plus the apparent effect of the Anastasia Formation has caused the main inlet channel to be located immediately adjacent to the southern margin of the inlet. On the open coast the trend for the past century has been one of accumulation on the north and erosion on the south side of the inlet (Mehta and Jones, 1977).

Hurricanes generally have a significant effect on all coastal environments, especially inlets. In 1964, Hurricane Dora created a breach in the narrow neck of Rattlesnake Island immediately landward of the inlet. This breakthrough caused a drastic change in the inlet hydraulics with more than 80 percent of the tidal prism being exchanged through this inlet and nearly all of the remainder being transported by the north arm of the Matanzas River. The breakthrough was scoured to more than 12 meters depth and generated a shoal in the Intracoastal Waterway.

Closure of the breakthrough was completed late in 1976 by the U. S. Army, Corps of Engineers. Another extreme change in hydraulics was affected with about 95 percent of the tidal prism being carried by the north arm of the Matanzas River and the remainder through the south arm (Mehta and Jones, 1977). At this time much of the north arm of the river was choked with sediment in the form of a huge flood delta. Mehta and Jones (1977) estimate that the inlet traps more than 5×10^4 m^3 of sediment per year. A channel to accommodate small boats was dredged through this sediment in early 1977. Since that time there has been a slow but noticeable seaward migration of large sediment bodies. This migration rate has apparently decellerated as equilibrium conditions are approached.

Sediments in, and adjacent to, the inlet were studied by Brunson (1972) who analyzed 32 samples from several environments. Because of the great local variability and the small number of samples from the inlet itself (8), it is not possible to reach any meaningful conclusions from this data. Shell content ranged from 22-87 percent in the inlet with substantially lower values for the beaches. Inlet samples were coarsest of the environments sampled and showed great variation in sorting values (Brunson, 1972). Recent studies of sediment and bedform distribution (Lee, 1980) and sediment transport (Gallivan and Davis, 1980) provide detailed information on these parameters as well as their relationships to inlet morphology and processes.

FIELD STUDY

A comprehensive field study was conducted at Matanzas Inlet from July 22 to August 25, 1978. The field party consisted of R. A. Davis and W. T. Fox with the assistance of five students plus B. Brenninkmeyer and a group of four students from Boston College. The latter group was conducting a related study adjacent to the inlet with emphasis on suspended sediment, wave parameters, and currents in the surf zone. A brief

experiment utilizing the realtime, on-line spectral analysis system developed by L. Gerhardt (Renselaer Polytechnic Institute) was also interfaced with the project.

The field study under the present contract consisted of various time series approaches to data collection as well as student research projects which supplement the primary effort of the study (Gallivan, 1979; Seifert, 1979; Sheridan, 1979; Lee, 1980). Process data included tidal current speed and direction, longshore current speed and direction, wave height, wave period, and offshore wave data. This was supplemented by sediment transport and bedform studies in the inlet. Weather data were collected from the NOAA weather station at nearby Marineland (Figure 1) and tide data were taken from a guage under the south end of the bridge over the inlet. In addition, the inlet and the adjacent vicinity was mapped in detail.

An array of recording current meters (General Oceanics, Model 2010) was placed in the inlet mouth with data recorded at 15 minute intervals. The meters were moved at about 7-10 day intervals in order to cover the desired areas of the study site (Figure 2). Various malfunctions of some meters resulted in no data collected from about half of the instruments deployed. In order to supplement these current data, drogues were traced through the inlet at various tidal stages and a Marsh McBirney electromagnetic meter was used over a tidal cycle at each of the marginal flood channels.

Process data were obtained from each of four sites along the beach; two on either side of the inlet mouth. These are locations R and O on the south and B and E on the north of the inlet (Figure 2). Longshore current speed and direction, and breaker height were measured at each of these sites at least four times each day throughout a lunar tidal cycle. Measurements were taken at predicted times for high, mid-ebb, low, and mid-flood tidal stages. Wave period was measured at location R.

Beach profiles were surveyed at each of six locations (Figure 2) on both sides of the inlet mouth at weekly intervals over the study period. Detailed morphology of the entire inlet and adjacent coast was surveyed using a combination of fathometer traces (Ratheon Model 719B) and a surveying transit.

Inlet Morphology

General morphology and configuration of Matanzas Inlet is similar to the model proposed by Hayes (1975) for mesotidal inlets. The inlet appears to have a morphology which depends on significant contributions by both tidal currents and waves. The Matanzas River, which services the inlet, takes an abrupt bend northward behind Anastasia Island. This results in the asymmetry of the flood delta (Figure 3). The river channel splits around the tidal delta with an ebb shield developed on the distal portion (Figure 4a). Ebb spits are formed on the edge of the flood delta adjacent to the channels (Figure 3). The main inlet channel in the throat is displaced to the south side of the inlet where it is stabalized by the bridge footings and also by the Anastasia Formation which crops

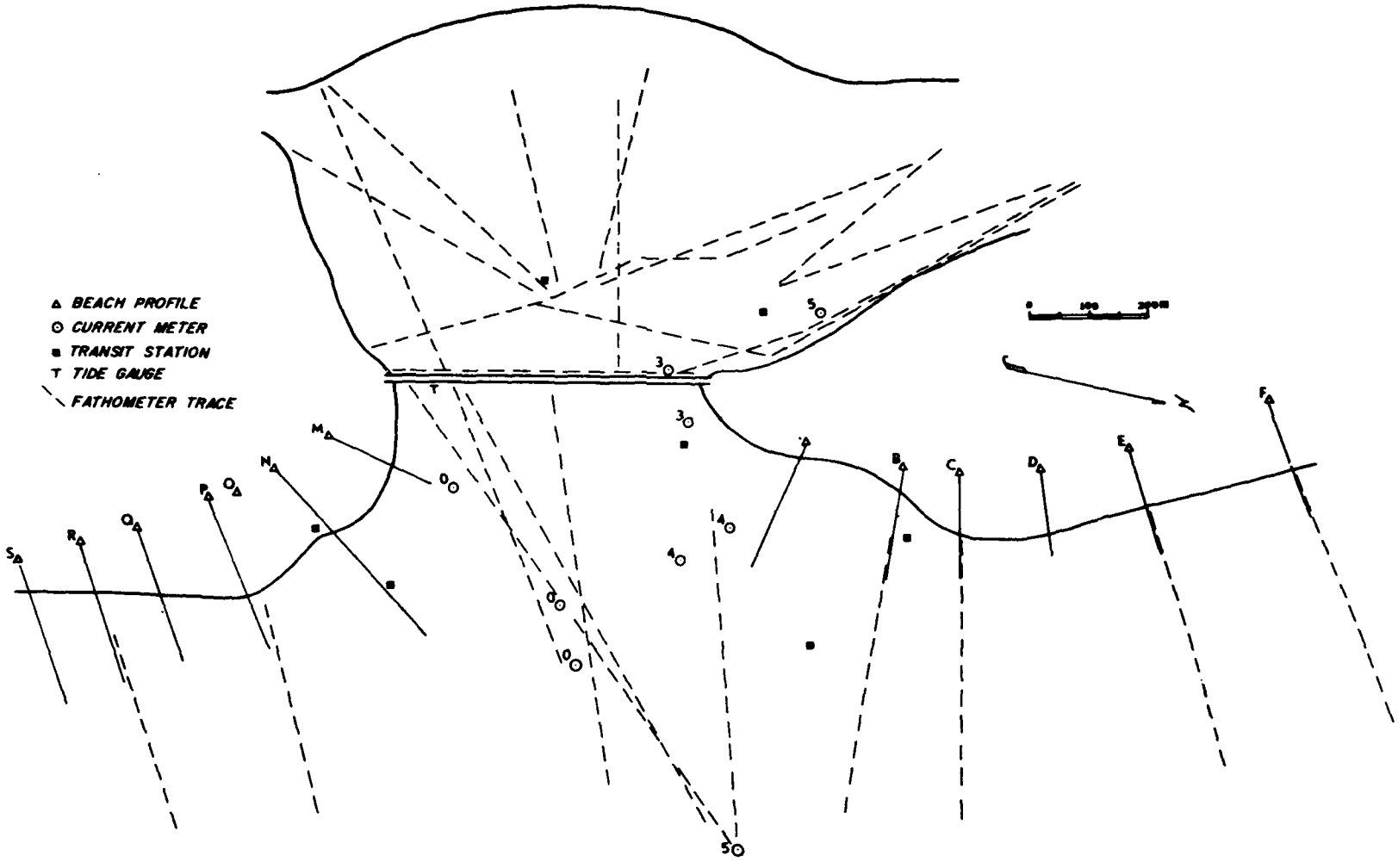

Figure 2. Map showing locations of various types of data collection at Matanzas Inlet.

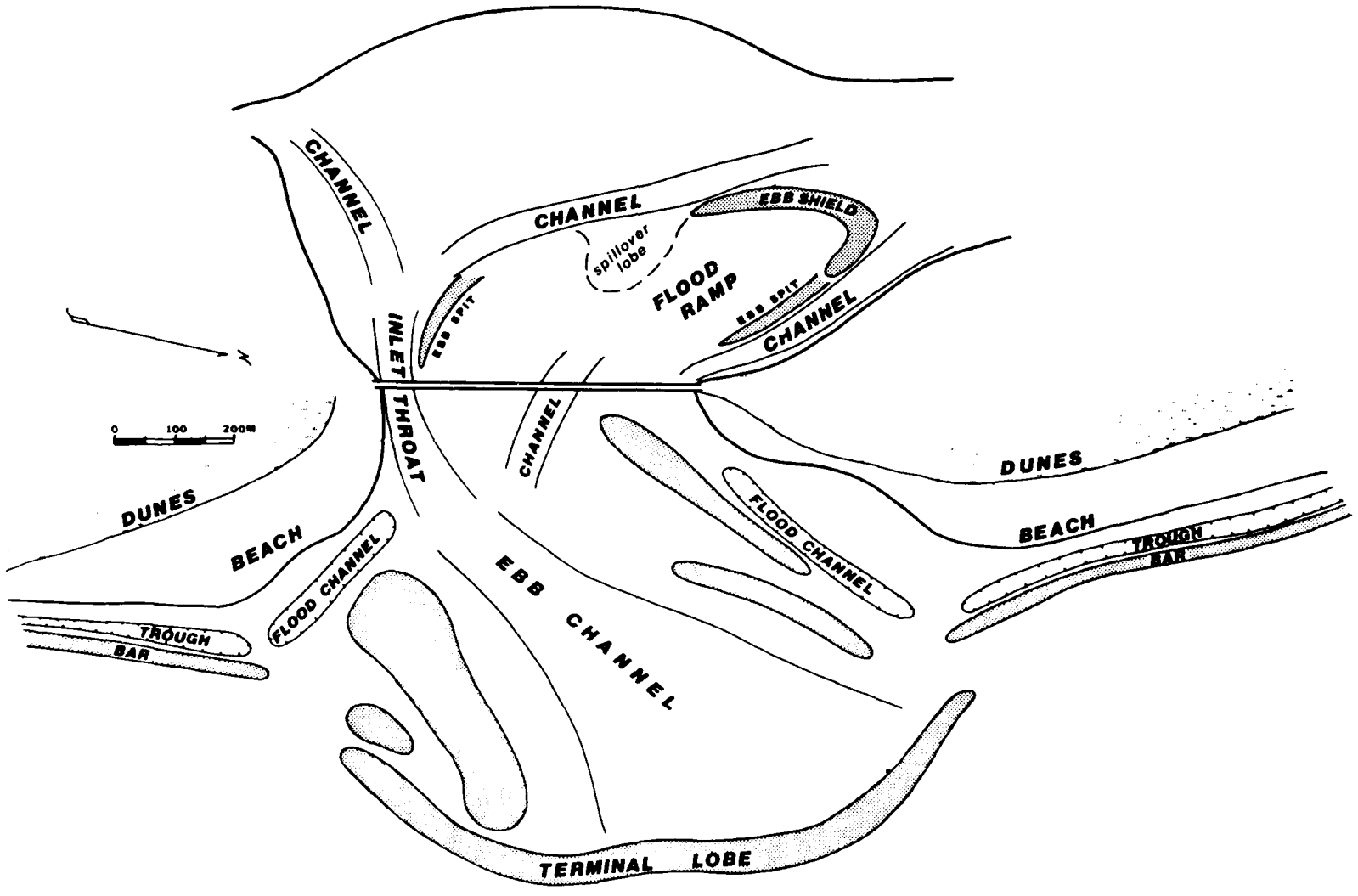

Figure 3. Major morphologic components of the Matanzas Inlet system.

out along the south side of the inlet.

The ebb delta shows morphology typical of mesotidal inlets (Hayes, 1975). The main ebb dominated channel is rather central in its location and has smaller, lateral flood dominated channels (Figure 3). These two channel systems are separated by elongate, channel-margin linear bars which are intertidal (Figure 4b). The seaward limit of the ebb delta is marked by an accurate terminal lobe which is a wave formed feature and is slightly subtidal at low tide. Although this terminal lobe is shoal throughout its extent, there is a slight saddle seaward of the ebb channel (Figure 5).

The deepest part of the inlet is the throat of the channel under the highway bridge where it exceeds 6 m. It shallows to less than 3 m in both the landward and seaward directions (Figure 5). The marginal flood channels are of different depths; the one on the south side is intertidal whereas the one on the north side is greater than a meter in depth at low tide. The dominance of south to north longshore current during the study period was probably a significant factor in this difference.

Historical Aspects

Fairly accurate maps of Matanzas Inlet date back to 1765. Since that time there has been a consistent and marked southerly migration of the inlet with the throat being located against the south channel (Mehta and Jones, 1977). Although the southward migration has been consistent, there have been different morphologies displayed by the tidal sediment bodies. Numerous sets of aerial photographs dating back to 1942 show these variations and indicate that the 1978 morphology (Figures 4 and 5) is comparable to that of 1942. During both times the main ebb channel seaward of the highway bridge is oriented to the northwest (Figure 3) and terminates at or just to the north of the north end of the bridge. In all other photographs this main ebb channel turns sharply to the north and enters the open Atlantic several hundred meters to the north of the end of the bridge. Extreme examples are in 1968 and during the field study of 1977 (Fox and Davis, 1977).

During January, 1977, the main channel crossed the terminal lobe of the ebb delta about 400 m north of the end of the bridge (Figure 6) or at location C of the summer study of 1978 (Figure 2). It should be noted however that shallow channels crossed the terminal lobe in January, 1977. A comparison between the general morphology and bathymetry of January, 1977 (Figure 6) and the summer of 1978 (Figure 3 and 5) shows additional differences although the deep channel in the inlet throat was similar in location and configuration during both times. In 1977 there was a deep hole (>7m) just seaward of the bridge and adjacent to the main channel (Figure 6). This area was only slightly subtidal during the 1978 field study (Figure 5) as the result of seaward migration of the large shoal area that was just landward of the bridge in 1977. A vertical accumulation in excess of 6 meters took place in 18 months.

Considerable erosion took place on the north bank of the inlet where a sediment accumulation of more than 100 meters in width was removed and

Figure 4a. Oblique aerial photograph of Matanzas Inlet at low tide looking southwest across inlet; Intracoastal Waterway and marsh.

Figure 4b. Oblique aerial photograph of Matanzas Inlet at low tide looking northwest up the Matanzas River with the Intracoastal Waterway on the left.

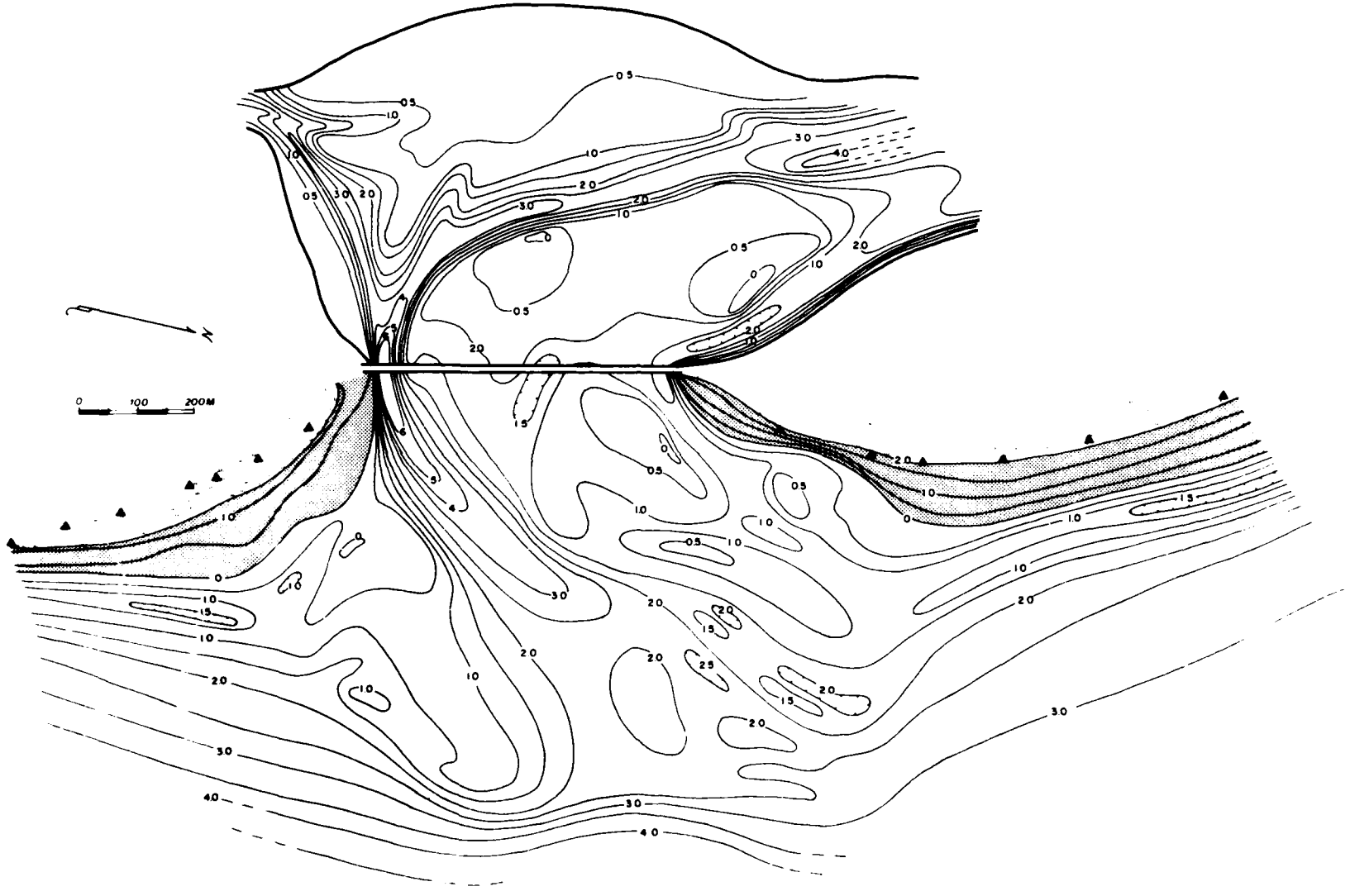

Figure 5. Bathymetry at Matanzas Inlet for summer, 1978. Contour interval is 0.5 m. Stippled area represents the beach.

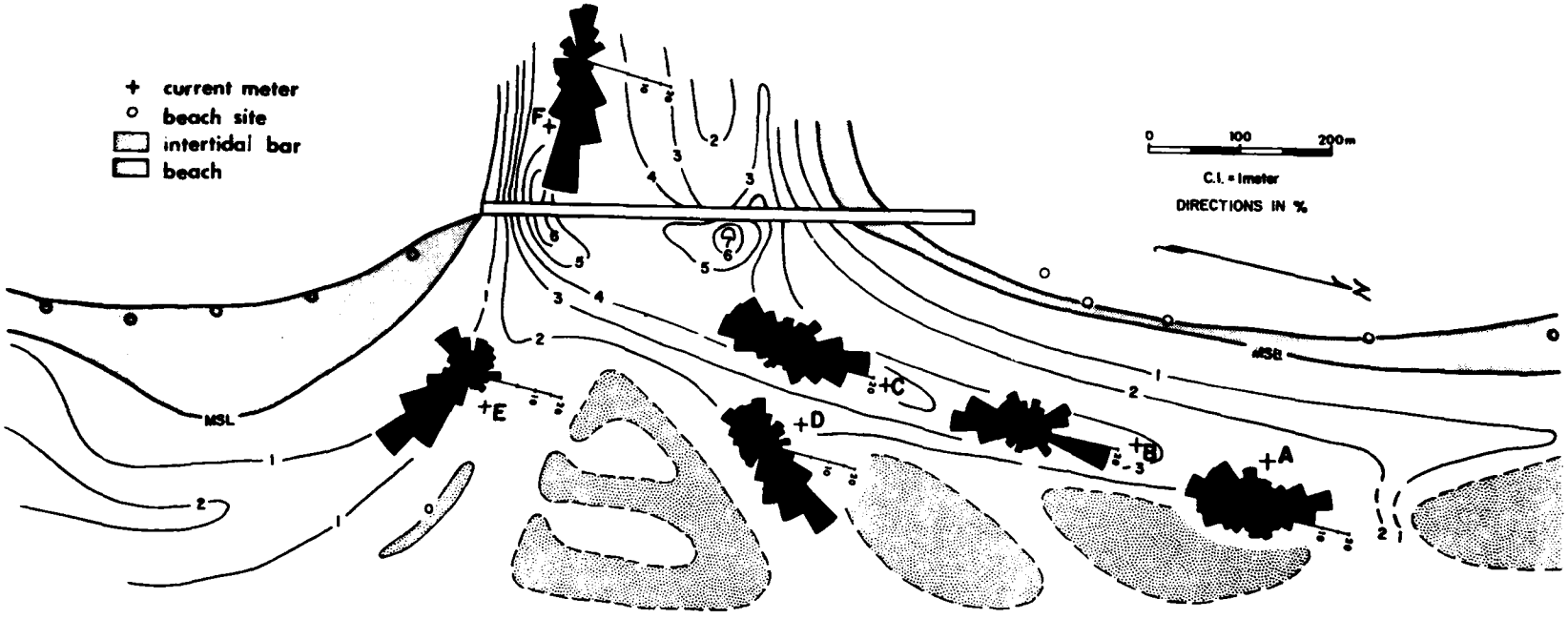

Figure 6. Configuration, bathymetry and current direction data at Matanzas Inlet, January, 1977.

a small channel developed (compare Figures 5 and 6). Most of this sediment was apparently transported seaward and filled in the seaward portion of the main channel as it existed in January, 1977.

The main ebb channel during 1977 exited the ebb delta near the position of current meter A, whereas in the summer of 1978 it exited at the position of meter D (Figure 6). Undoubtedly the major changes in morphology were in response to the changes in inlet hydraulics initiated by the combination of closing the breakthrough on Rattlesnake Island and the dredging in the flood delta area. The seaward movement of great quantities of sediment apparently forced the main ebb channel to a more central position in the ebb delta.

PROCESSES

Tides

Tide ranges at Matanzas Inlet are from about 100 cm to near 180 cm over the lunar cycle. This places the area in the microtidal range of Davies (1964) although inlet morphology is strikingly similar to a wave-dominated mesotidal inlet as described by Hayes (1975) and Boothroyd (1978). General tidal environment is semi-diurnal with moderate diurnal inequality (Figure 7).

Because Matanzas Inlet is not one of the sites for which predicted tide data are available, it is necessary to modify data from the tables (NOAA, 1978). Mehta and Jones (1977) used tide data from the pier at Flagler Beach, 25 km to the south, to characterize open tidal conditions. They determined the spring range at that site to be 173 cm which closely agrees with the range as measured under the highway bridge over the inlet. Predicted tides for Matanzas Inlet were plotted using 80 percent of the predicted values from standard tide tables (NOAA, 1978). This showed good agreement with Mehta and Jones' (1977) limited data and the data recorded under the bridge. Predicted tide range shows a marked difference in spring range between full moon and new moon (Figure 7).

Tidal level data were recorded at the inlet throat by an 8-day, float type level in a stilling well. The gauge malfunctioned on several occasions and the net result was only about 14 days of data during the 30-day study period. Tidal curves showed no significant deviation from predicted curves except during the last two days of operation (August 22 and 23). This was the period of brisk northeasterly wind and somewhat higher than normal waves. About 20-25 cm of set up was recorded during this period as water was pushed into the estuary.

Weather Data

Weather data utilized in this project include barometric pressure (Bp), wind speed (Ws), and wind direction (Wd). This information was obtained from the NOAA weather station located at Marineland, about 3 kilometers south of Matanzas Inlet (Figure 1). Because of a malfunction in the weather vane during part of the study, wind direction data were

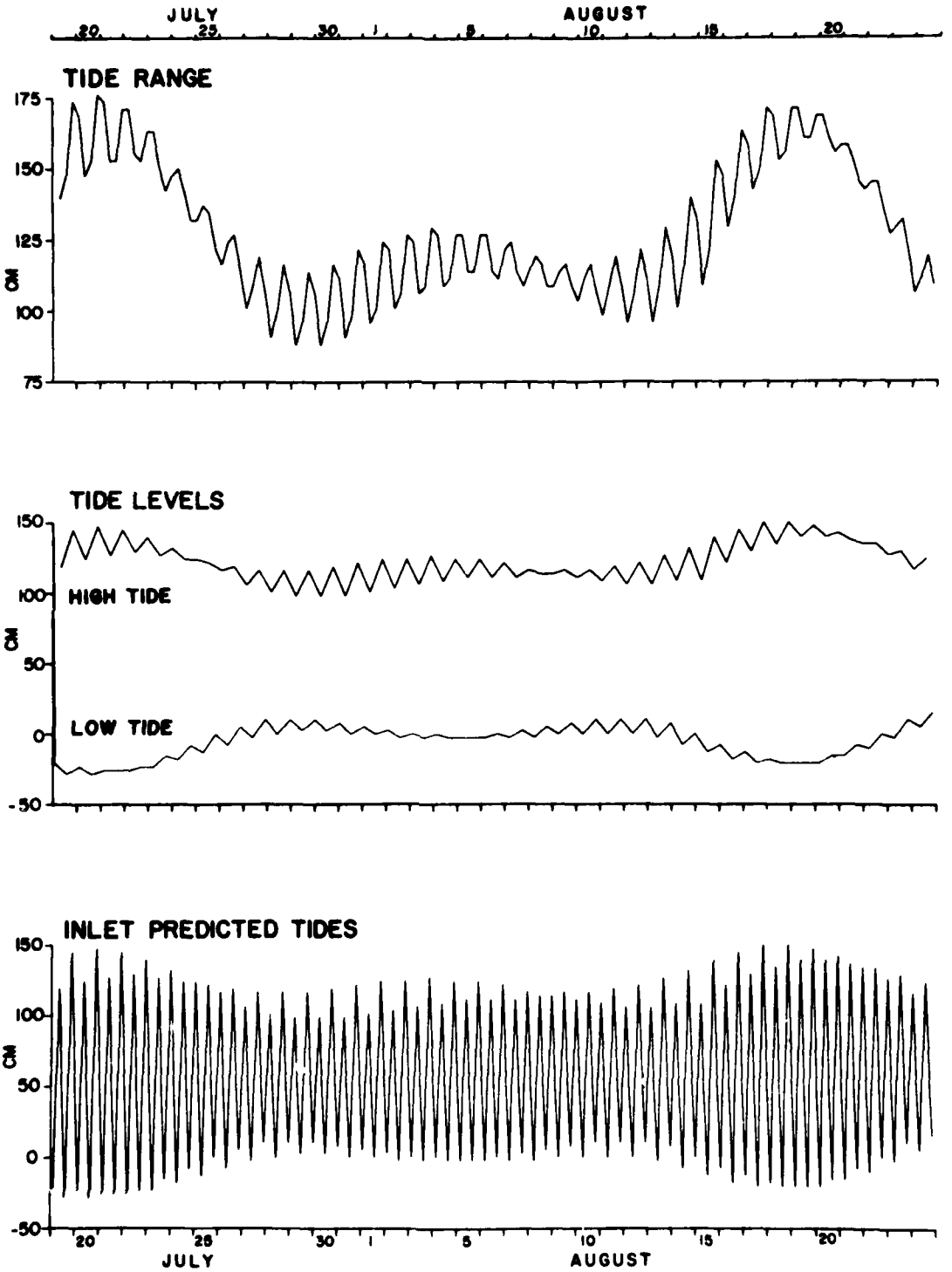

Figure 7. Predicted tide data for Matanzas Inlet, Florida, during the study period. Predicted records are based on a factor of 0.80 as compared to St. Augustine Inlet.

used from the Jacksonville weather station. Although this is a long distance from the study site the directional data are comparable to that from the Marineland station.

Summer weather along the Florida coast is characterized by quiescent conditions with prevailing winds from the southeast to southwest. Occasional local afternoon thunderstorms move from the mainland across the coast in a seaward direction but major frontal systems are generally lacking. The study period was fairly representative of typical summertime weather patterns. Barometric pressure range was only 7.5 millibars during the 28-day time-series study. No prominent frontal systems passed over the area and winds were generally steady at between 5 and 12 knots (Figure 8). Short periods of high wind speeds occurred several times during local thunderstorm activity. Although wind speeds were typically about 25 knots during these events they were not sustained and had no significant effect on coastal processes.

Wind direction was dominated from the southeast to southwest throughout nearly all of the study period. There was a minor but significant deviation from this pattern during the last few days of the study period. During this time wind direction was from the northeast with speeds somewhat elevated above normal (Figure 8).

Although more extreme events would have provided a better spectrum of conditions, the sustained quiescent period provided a good and relatively simple set of conditions for identifying effects of tidal conditions in the inlet transition. It is anticipated that this baseline data can be interfaced with data from previous and similar studies in order to determine storm effects in this environment.

BEACH SITE OBSERVATIONS

A time-series study of beach processes was conducted over a 28-day lunar cycle from July 27 through August 24, 1978. Measurements of the longshore current speed and direction as well as breaker height were taken at each of four sites, two on either side of the inlet mouth. Sites chosen were at locations C and E on the north and O and R on the south side of the inlet (Figure 2). Measurements were taken at predicted high, mid-ebb, low, and mid-flood stages every day. In order to obtain synoptic data two teams took measurements, one on each side of the inlet. In addition to longshore current and breaker height, the wave period was also measured for at least one location during most visits.

Waves

During the study period the breaker height (Hb) ranged from 16 cm to 105 cm. This is a modest range and is due to the absence of significant storm activity during the study period. Offshore, deep water waves were measured by a pressure transducer in 7 meters of water a distance of one kilometer from shore. The pressure transducer is located opposite

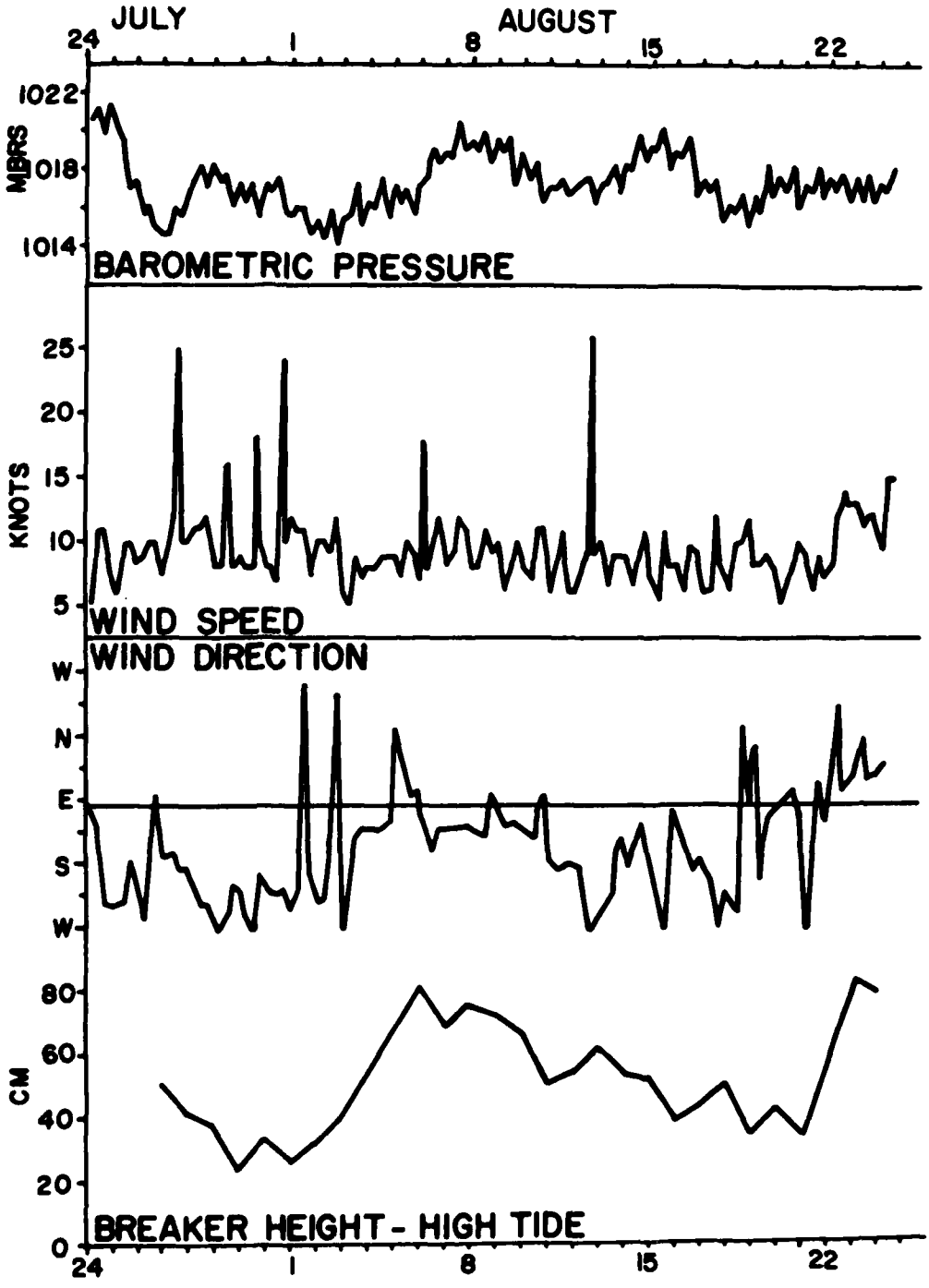

Figure 8. Temporal distribution of barometric pressure, wind speed and direction as compared to high-tide breaker height, Matanzas Inlet.

the University of Florida's Whitney Research Laboratory at Marineland (Figure 1). Significant wave height was recorded twice each day and shows the expected correlation with breaker height (Figure 9).

There is little difference in breaker height when mean values are plotted by location and by tidal stage (Figures 10, 12 and 13). There is distinct similarity and consistency in these data with only location E showing slight but consistently higher values than other sites. Lowest values overall are at location B which is expected due to the sheltering effect of the terminal lobe in the prevailing wave approach from the southeast. Comparison of these data with those collected during the brief study in January, 1977 shows a somewhat similar pattern (Figure 10 and 11). During the January study mean values for each tidal stage were similar or less. The most striking difference in the trends of the plots is the apparent effect of tidal stage on breaker height. The 1977 data show up to 30 cm differences between breaker height at low tide as compared to high tide for several of the locations. The reason for these differences is the sheltering effect of the intertidal shoals to the north of and opposite the inlet mouth (Figure 11). Data collected by Finley (1976) at North Inlet, South Carolina, shows similar sheltering effects.

Longshore Currents

Measurements of longshore current speed and direction showed considerable range in speed and direction with respect to tidal conditions and to a lesser extent with time. Currents ranged from 100 cm/sec to the south to 125 cm/sec to the north, however, this range is misleading. In order to properly assess the temporary and spatial distribution of longshore current values, one must isolate the individual locations and also the tidal stage. The latter is of particular importance because of the retardation or reinforcement of longshore currents by tidal currents flowing in or out of the inlet.

A summary of longshore current data is shown on Figure 10. Some interesting and important generalizations can be made from these data. Because of the bidirectional nature of longshore currents it is not meaningful to consider the mean values of current speed for each location. For example, location B exhibited great variability during high tide conditions, however the mean current speed is only 0.4 cm/sec. It is therefore appropriate to consider each site in relation to the tidal stage as well as looking at tidal stage in general. The greatest overall variation in longshore current occurs at high tide. Not only did each site exhibit the greatest variability but the mean range at high tide (161.8 cm/sec) was nearly twice that for low tide (82.0 cm/sec).

Longshore currents from each of the four beach sites show that at the distal locations there is nearly complete correspondence in current direction with the expected direction at the distal sites (E and R) based on wind direction and angle of wave approach. Throughout all but the last few days, wind and waves were from the south and southeast thereby generating northerly (positive) currents. A few readings taken at predicted

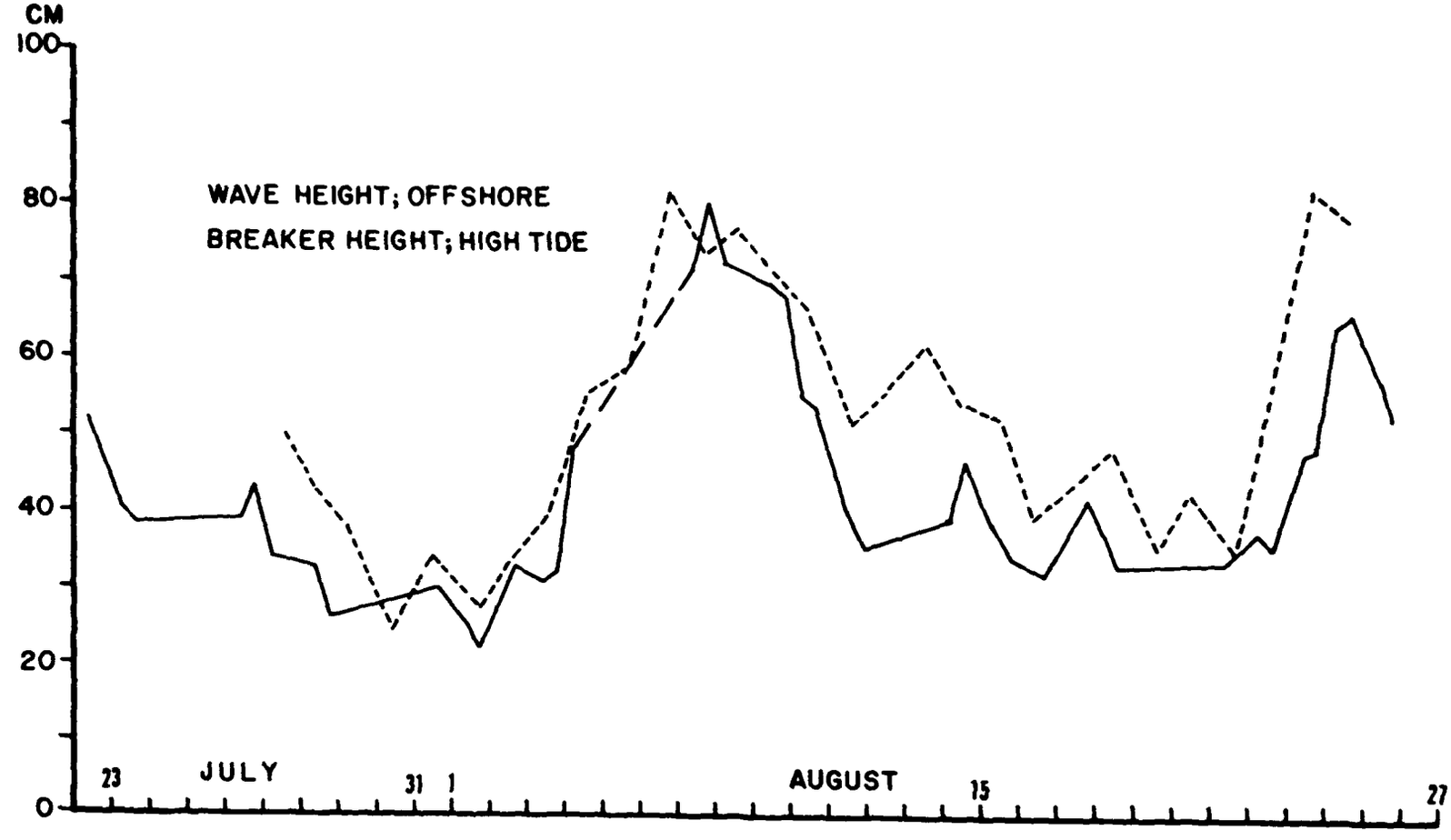

Figure 9. Mean breaker height at high tide compared to offshore wave height. Offshore values are significant wave height as measured in 7 meters of water at a distance of one kilometer from the shore and 2 kilometers south of Matanzas Inlet at Marineland.

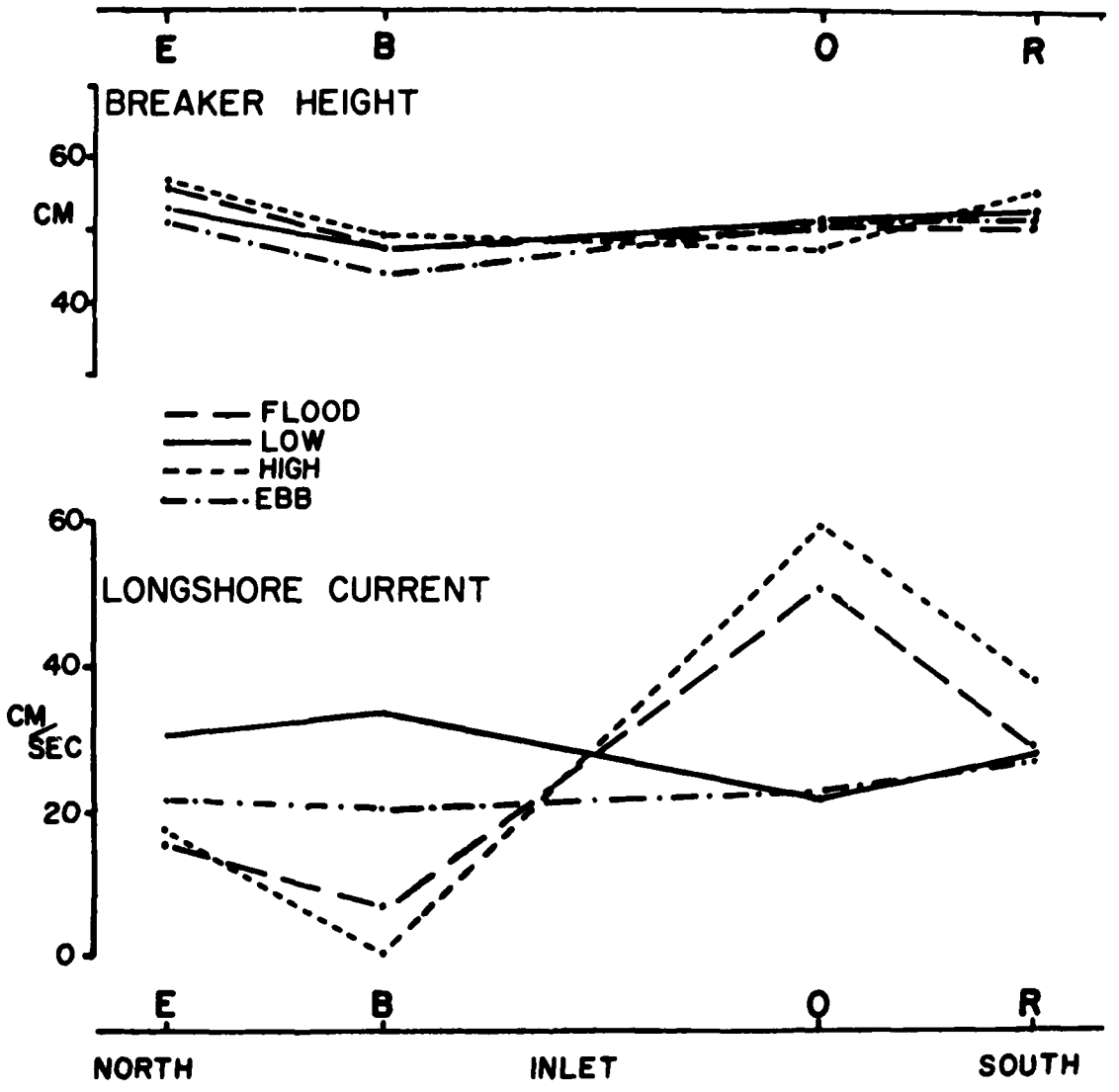

Figure 10. Summary plot of mean breaker height and longshore current values during the study period at each beach location. Compare with Figure 9.

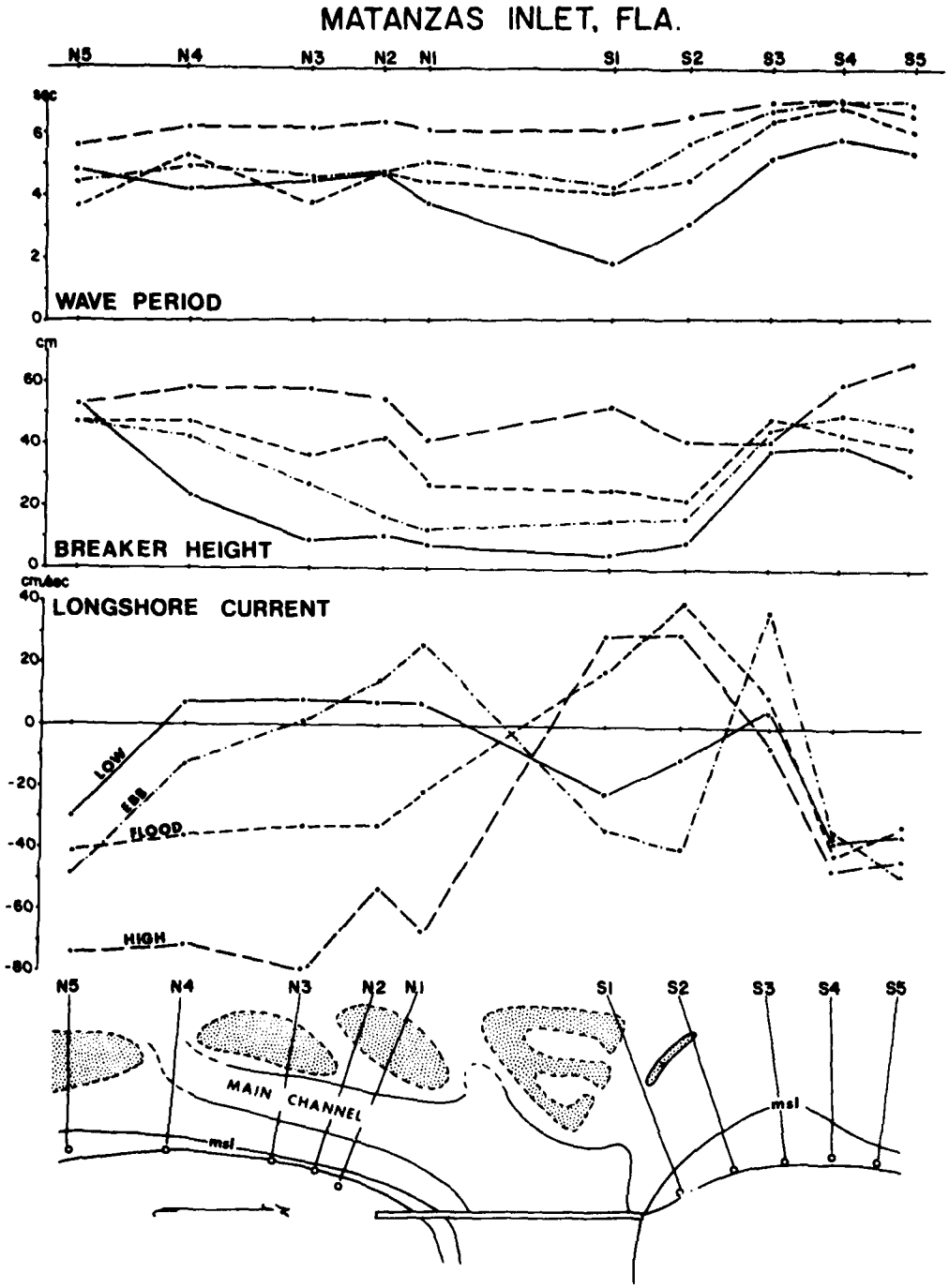

Figure 11. Values of wave period, breaker height and longshore current at various tidal stages for each of nine stations during January, 1977 study period.

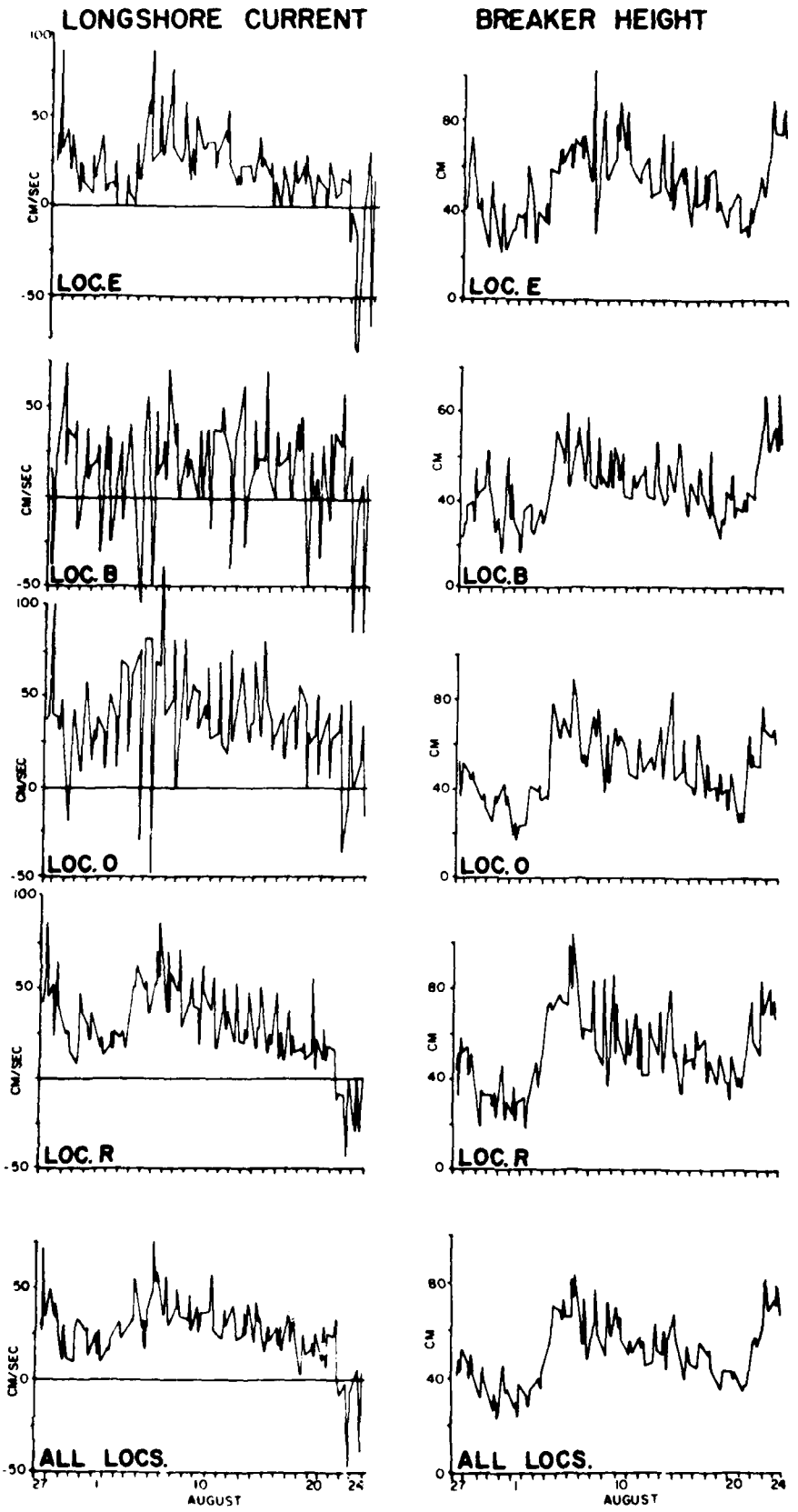

Figure 12. Observed values for longshore current and breaker height by location and as mean values. Negative values indicate longshore current is to the south. See Figure 3 for locations.

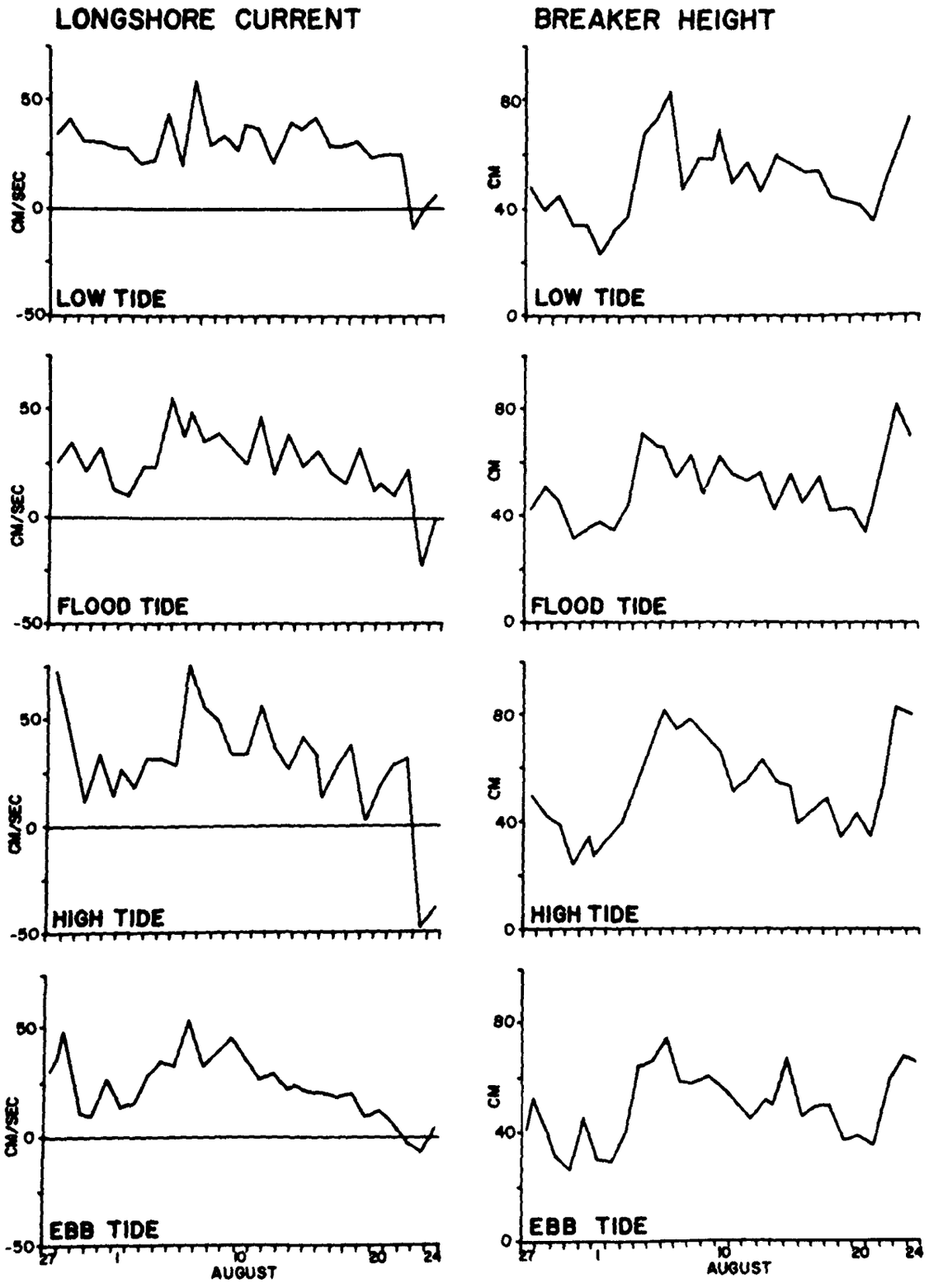

Figure 13. Observed values for longshore current and breaker height by tidal stage. Negative values indicate longshore current is to the south. See Figure 3 for locations.

flood and high tide stages do show some influence of tidal currents on longshore currents at these sites. The combination of flooding tides plus the shadow effect of the ebb delta gives rise to lower north-flowing longshore currents at location E than at location R (Figures 2 and 5). Similar but opposite effects were observed the last few days when northerly winds and waves generated south-flowing (negative) longshore currents.

This general pattern of the relationships between tide stage, location and longshore current is shown in Figures (10, 12 and 13). The northerly flowing longshore currents which persisted throughout the bulk of the study caused mean speed for the study period to yield positive values. Note that at the distal locations (E and R) there is little variation with tidal stage. This supports the premise that tidal currents are not having a marked effect on surf zone currents (longshore) at these locations. One can see however that at the distal sites the flood and high tide values are lowest north of the inlet (location E) and highest south of the inlet (location R). These data show that during predominantly north flowing longshore currents there is a general reinforcement of tidal currents on the upstream side (R) and suppression of the same currents on the downstream side (E).

Great modification of surf zone currents was found adjacent to flood channels (locations B and O). Flood and high tide stages show lowest values downstream (B) and highest values upstream (O) within the longshore current system. There was only marked variation of speed and direction in the proximal sites due to tidal cycles (Figure 10). Such relationships were expected, however their restricted extent was not.

INLET CURRENTS

Longshore and tidal currents converge at the mouth of Matanzas tidal inlet producing a complex pattern which varies with the tidal cycle and with meteorological conditions. Currents in the vicinity of the inlet were recorded with moored current meters and by tracking current drogues from shore positions. The moored meters were used to study the currents in a Eulerian framework in which instantaneous speed and direction are recorded at a fixed location through time. The time-series data produced by an array of moored meters gives a record of changes in velocity through several tidal cycles at different locations in the inlet. In order to determine velocity gradients between meters, current drogues were released within the inlet and tracked by triangulation. The drogue studies result in Lagrangian streamlines which are plotted on a map with velocities along the streamlines. Drogues were released at different times in the tidal cycle to plot current vectors under different tidal regimes. By combining the Eulerian and Lagrangian data from the meters and drogues, it was possible to construct a model of the current pattern in the inlet as a function of time and space.

Current Drogue Studies

Twenty-six biplane drogue paths were tracked from the highway bridge

to determine the speeds and paths of currents in the inlet and along the north and south beaches (Figures 14 and 15). Thirteen drogues were released during ebbing tide, eleven during flood and two when the tide was reversing from flood to ebb. Most of the drogues were released and recovered from a boat within the throat of the inlet, but some were released from the bridge and drifted over the terminal lobe. Others were released along the beach and allowed to drift into the inlet.

For tracking the drogues, a 500 meter baseline was laid out on the bridge with survey stations marked at 50 meter intervals. Two transits were set up 250 meters apart on the bridge and the drogues were tracked by triangulation. After a drogue was launched, a radio was used to coordinate the time of the sightings at one minute intervals. Each drogue consisted of a pair of metal fins mounted on a rod and suspended beneath a styrofoam float. The fins were 30 cm square, with the center of the fins half a meter below the water surface (Sheridan, 1979).

The drogues are identified by the starting time from the last high or low tide (Figures 14 and 15). The pattern of trajectories for drogues released during flood is shown in Figure 14. In the surf zone, the drogue traveled northward at about 40 cm/s. In the south flood channel, the speed increased to about 60 cm/s and reached 80 cm/s in the main ebb channel.

The 15 drogues released during the ebb tide are plotted on Figure 15, with two runs that reversed direction when the tide turned from ebb to flood.

Four drogues released in the back of the inlet followed the same general path, but their speeds varied considerably. Those released early in the ebb cycle had speed of 30 to 35 cm/s. While those released near the end of the middle of the ebb cycle reached velocities of over 100 cm/s.

Two drogues were released from the bridge near the middle of the ebb and traced similar S-shaped paths (Figure 15). In the main ebb channel, the direction shifted to the northeast and velocity increased to about 70 cm/s. The speed dropped off to about 20 cm/s as the drogues moved across the swash bars.

Drogue runs in the north channel reached speeds of 100 cm/s near the bridge, but gradually slowed down from 70 to 30 cm/s in the north flood channel.

During the ebb cycle, the current moved through the constricted inlet throat and reached the highest velocity at mid-ebb in the deep channel. On the ebb delta, channels became shallow, currents diverged, and speed decreased.The trajectory of drogues also changed progressively in the ebb cycle. Early in the ebb when water level was high, the flow radiated out from the inlet throat. In mid and late ebb, the flow was more confined by the channels and bars. The longshore current from the south forced the swash bars into the channel and shifted the currents to the north.

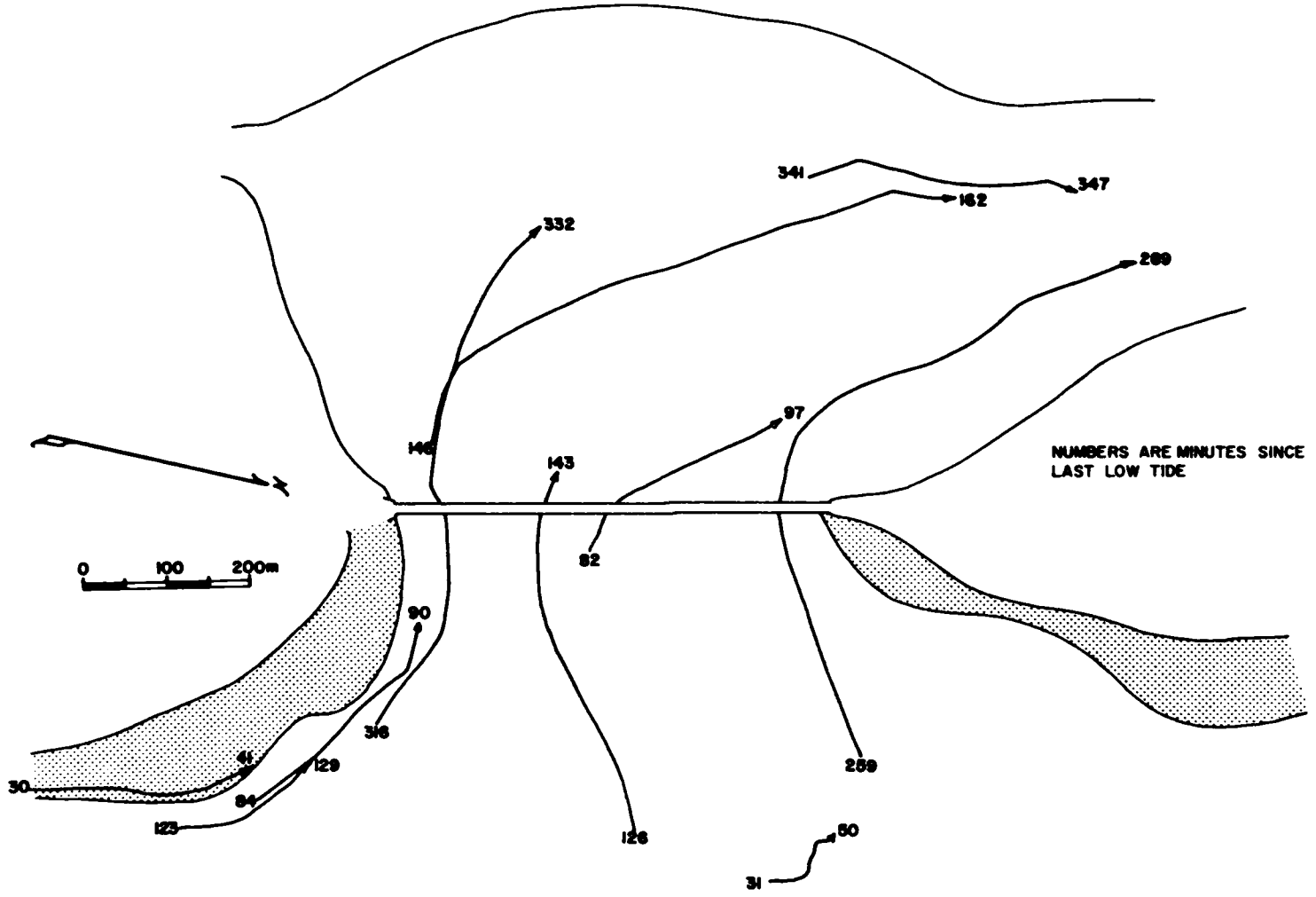

Figure 14. Drogue runs during flood tide conditions.

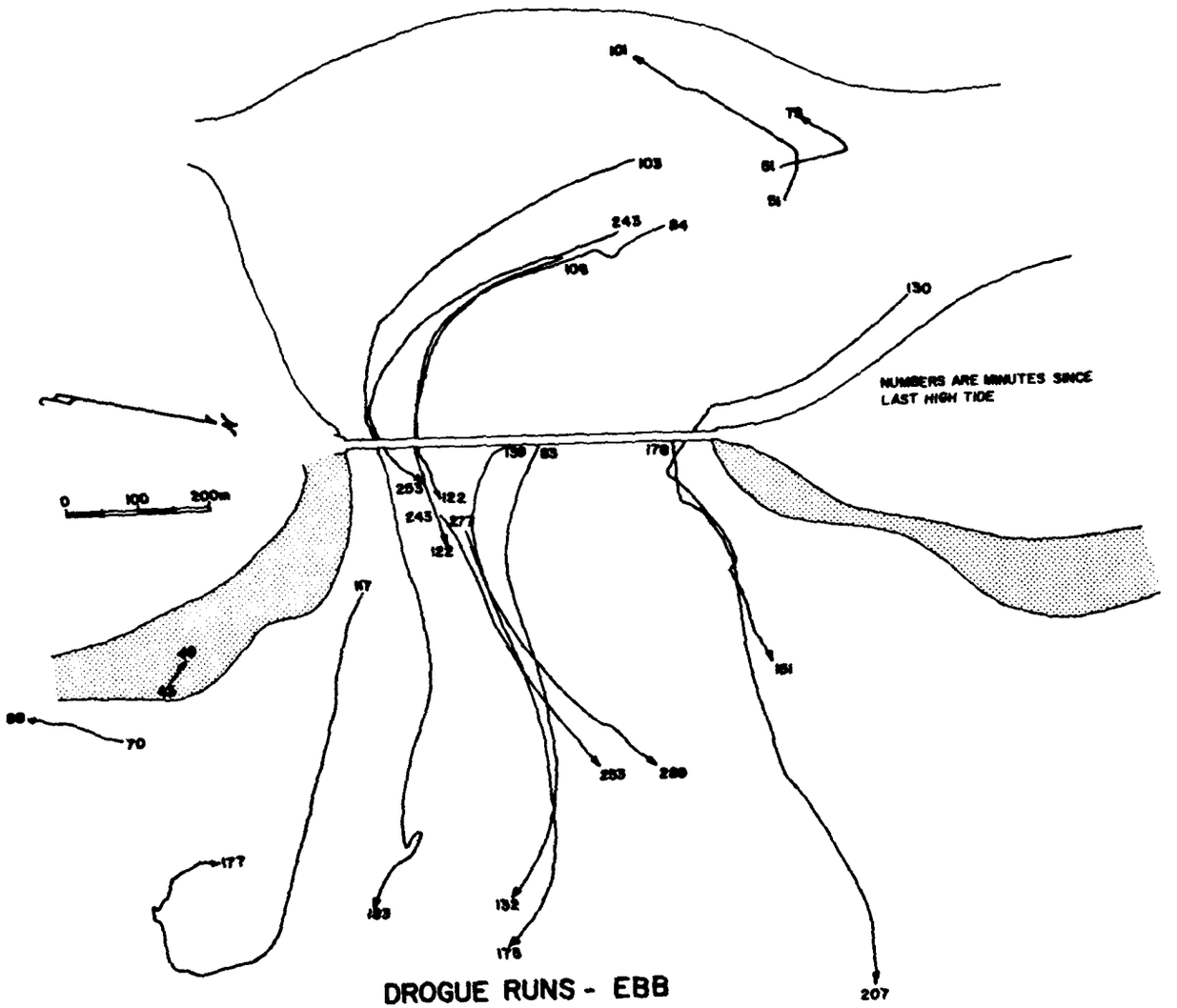

Figure 15. Drogue runs during ebb tide conditions.

Flow Meter and Electromagnetic Current Meter Data

A March-McBirney electromagnetic current meter and five digital flow meters (General Oceanics, Model 2030) were used to measure current speed and direction from the bridge and in the flood channels flanking the inlet. The flow meters were deployed at several stations simultaneously to get a synoptic view of the current pattern through a tidal cycle for a small portion of the inlet. The meter array was then moved to another location to collect data over a later tidal cycle while continuous data were being recorded by the moored meters.

A current profile across the bridge was constructed from data collected between 6 a.m. and 6:15 p.m. on August 22, 1978. Five stations were established at 100 meter intervals across the bridge starting 50 meters south of the north bridge abutment. Current was measured by a digital flow meter which was lowered from the bridge and submerged one meter below the surface for 100 seconds. The meters were lowered once every half hour during mid-ebb and mid-flood, at 15 minute intervals during the hour before and after changing tides.

The velocity data from the bridge study are contoured on a time-distance diagram (Figure 16). The measurements started about one hour before low tide and continued through high tide and back to low. During the flooding tide, the maximum speed in the north flood channel (Station 350), the flood currents also peaked at 10:20 a.m., but the maximum current velocity was only 83 cm/s. At Station 450 near the south margin of the ebb channel, the maximum flood current was 64 cm/s at 10:20 a.m. The maximum ebb current of 118 cm/s occurred in the ebb channel in location 450 at 4:40 p.m. At location 350 the peak ebb current velocity was only 63 cm/s, and in the north flood channel (location 50), the maximum ebb current was 72 cm/s.

The time of the maximum ebb current at the north side of the inlet was about half an hour earlier than the maximum in the ebb channel. In general, the ebb current was deflected to the south side of the inlet and the flood current was greatest on the north side. Although this could be considered a manifestation of the Coriolis effect with currents deflected to the right in the northern hemisphere, it is more likely a result of the channel configuration. The ebb channel swings around a meander bend as it moved through the inlet. Therefore, the ebb current is forced to the outside of the bend as the current moves toward the ocean. The flood current is not constricted to a channel and is more influenced by longshore current. Therefore, the flood currents are similar on the two sides of the bridge study, the longshore currents were coming from the north, while during most of the study, the longshore currents were coming from the south.

Velocity measurements were made through a tide cycle at 9 stations in the south flood channel on August 10, 1978 (Seyferth, 1979). The data suggests that the term "flood channel" was aptly chosen, especially for the south flood channel. The duration of the flood stage was longer than the ebb in both channels, but was more pronounced in the south flood channel. In the south channel, the tide currents reversed less than half an hour after low tide and between one and three hours after high tide with a mean

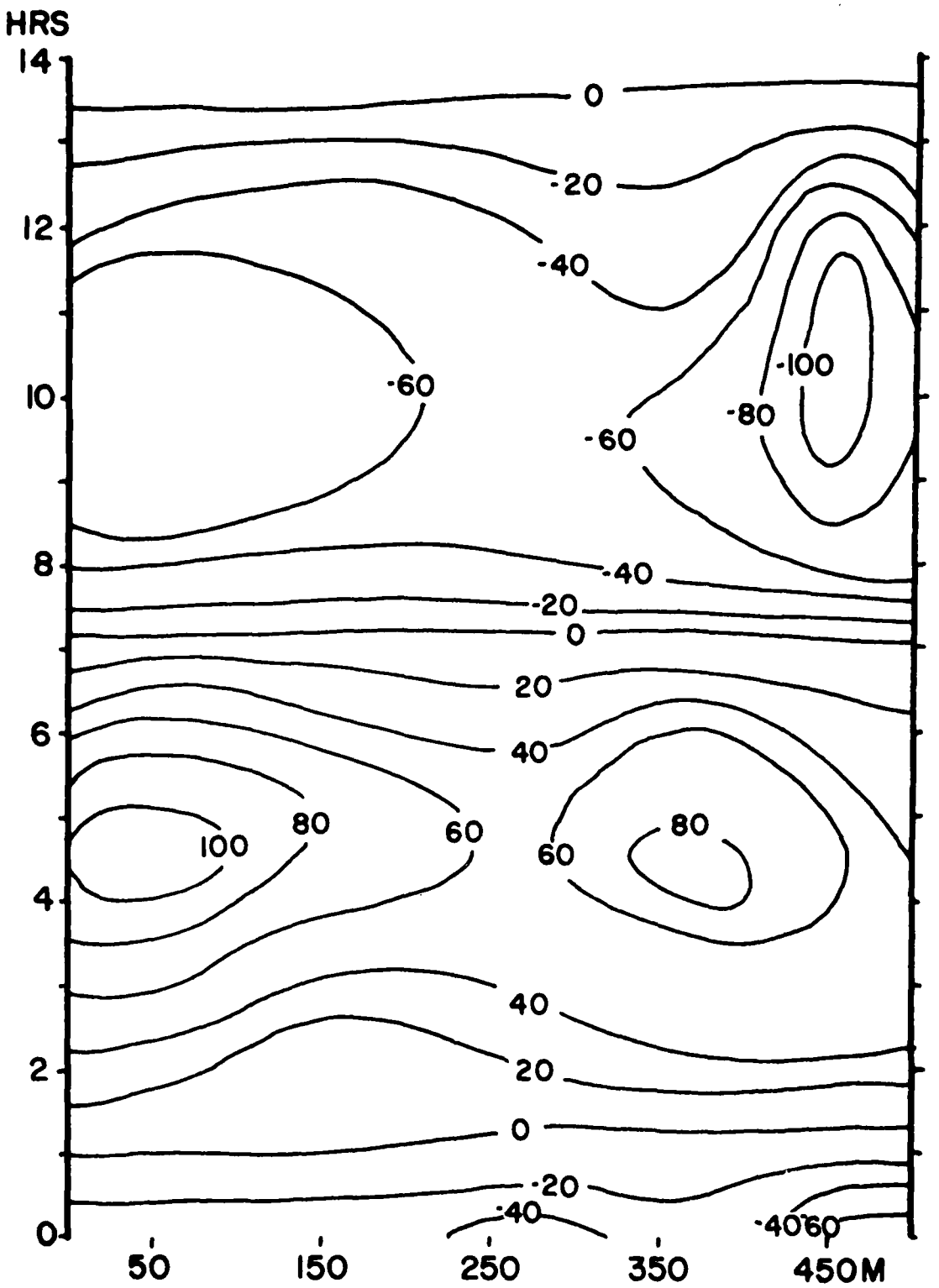

Figure 16. Time-velocity plot of surface currents measured through a complete tidal cycle from the bridge over Matanzas Inlet. Data were collected at 100 M intervals as shown along the base of the diagram. Contour interval is 20 cm; positive values are flood currents and negative values are ebb currents.

delay at the 9 stations of 1.7 hours after high water. During slack water when the tidal current velocities were low and inertial effects were dominant over friction, the longshore current has its greatest impact (Mehta, 1978). With the strong longshore current from the south on August 10, the longshore current contributed significantly to the flood current in the south flood channel.

Five stations in the north channel provided ebb and flow velocities at half hour intervals on August 15, 1978 (Seyferth, 1979). Although the velocities were not as high in the north channel, it still showed evidence of flood dominance. In the south channel, four stations had maximum velocities and two had higher ebb velocities. Although the peak velocities showed no clear cut flood or ebb dominance the shape of the velocity time curves indicates the importance of the flood. The flood stage had relatively high currents with a maximum of about 120 cm/s over a longer period of time.

The tidal volume was computed at four cross-sections for the south flood channel and three cross-sections for the ebb channel (Seyferth, 1979). The volumes for two sections in each channel are listed in Table 1. The average flood volume in the south channel was about 1.35 times greater than the flood volume for the north channel. The longshore current flowing from the south supplemented the tidal flow on the south side. The flood-to-ebb ratio in the channels was 3.7 on the south side and 2.6 on the north side.

Table 1. Discharge volumes in thousands of cubic meters during ebb and flood tides in the south and north flood channels.

	South			North		
	A	B	AVG.	A	B	AVG.
Flood volume	32.0	34.0	33.0	25.0	24.0	24.5
Ebb volume	9.9	8.1	9.0	11.0	7.8	9.4
Flood/Ebb	3.2	4.2	3.7	2.3	3.1	2.6

Moored Current Meters

In January 1977, current speed and direction was determined for 6 meters (General Oceanics, Model 2010) moored for 5 days in the inlet mouth and along the adjacent shore (Figure 17). The three northern meters, A, B, and C, show a bimodal current distribution with a dominant flood mode heading into the inlet. The flow during flood is reinforced by the southward flowing longshore current. Meters D and E, located in the main ebb channel also have a bimodal distribution, but the ebb mode is larger. The ebb current at meter E is also influenced by the southward flowing

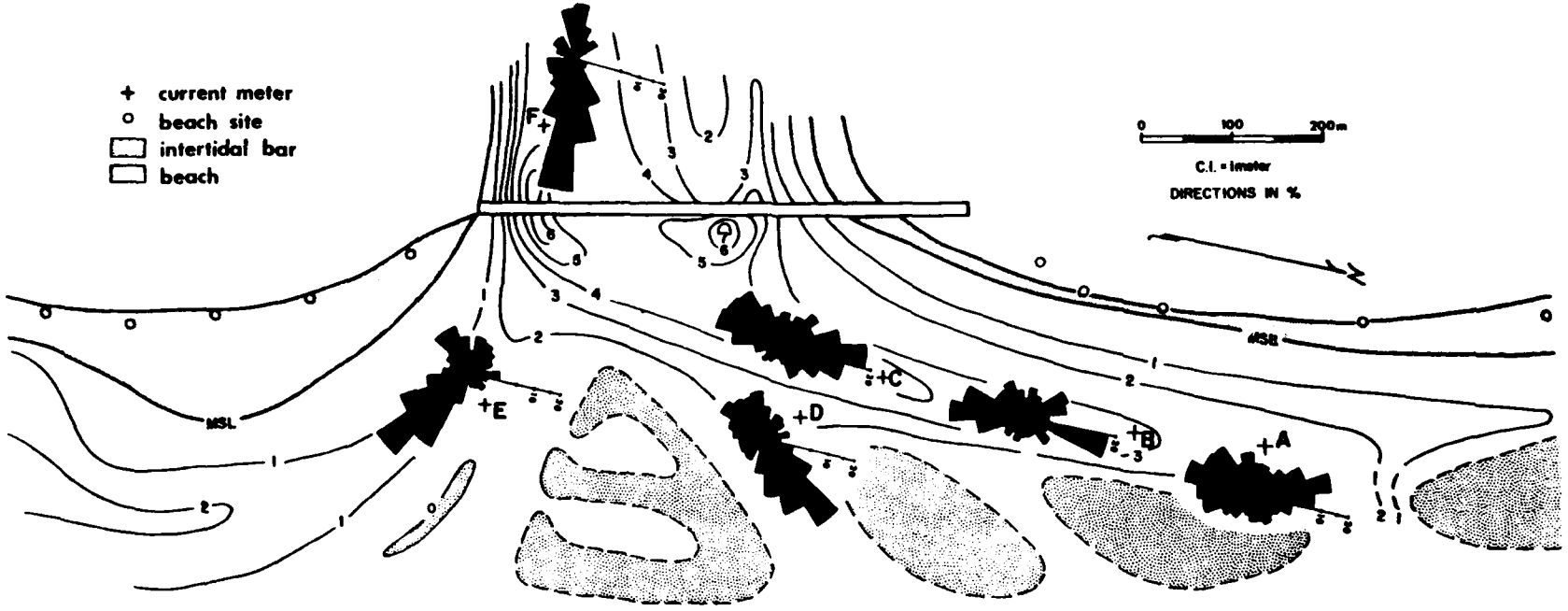

Figure 17. Rose diagrams showing current directions during January, 1977 study period.

longshore current. Meter F inside the throat of the inlet had an ebb dominance, but it was hung up during part of the recording interval. The rose diagram for January, 1977 (Figure 17) provides an interesting contrast with the rose diagram for August, 1978 (Figure 18). During the winter the longshore current is dominately from the north and the flood current on the north side of the inlet is strongest with ebb dominance on the south side of the inlet. In summer, the longshore current is from the south and the flood current on the south side of the inlet is strongest. The current roses for August, 1978 show a bimodal current direction for ebb and flood, but the ebb and flood currents 180° are not opposed (Figure 18). The bottom configuration and effect of longshore currents account for shift in the ebb and flood currents.

Velocity vectors

Velocity vectors are used to show how the speed and direction of the tidal currents vary during a tidal cycle. The velocity vectors are plotted with the baseline parallel to the bridge and the length of the vector proportional to the speed of the current (Figures 19, 20 and 21). The vectors are plotted at 15 minute intervals, the recording interval for the moored meters. The plots are marked with the flood direction (positive) into the inlet and the ebb direction (negative) flowing out to sea.

The velocity vectors for meter locations 3-1, 4-1, 0-1 on July 28 and 29 are given in Figure 19. Meter 3-1 is located under the bridge on the north side of the inlet, meter 4-1 is located in the flood channel on the north side of the meter 0-1 was moored near the seaward end of the ebb channel (Figure 2). Meter 3-1 shows a unidirectional flood current with some shifts due to wave action at low water. The velocity vectors during the ebb indicated a shift in current direction in a clockwise direction. Early in the ebb, the currents flow across the flood ramp and out to sea. Late in the ebb, the currents flow in the channel around the eastern margin of the ebb shield and across the inlet mouth. At meter 4-1, the ebb and flood currents are directly opposed and do not show a shift through time. At meter 0-1 in the ebb channel, the flood currents show a widely scattered pattern due to the strong influence of waves. The ebb current at meter 0-1 shows a clockwise shift in direction which is similar to the shift recorded at meter 3-1.

The velocity vectors for meters 4-2, 3-1, 5-1 and 0-2 on August 4 and August 5 are plotted in Figure 20. Meter 4-2, located in the north flood channel shows a very complicated vector plot. The general ebb and flood patterns are evident, but it is complicated by the local topography. At mid ebb, the shoal area adjacent to the north flood channel emerges and currents are restricted to the flood channel. When the shoal is submerged at mid flood, the currents flow over the shoal from the southeast, and waves sweep over the shoal. An eddy current may also be located near meter 4-2 which would affect the current directions. In early August, meter 3-1 remained in the same location and the vector plot is similar to that recorded in Figure 19. Meter 5-1 was located landward of the bridge in the channel adjacent to the flood ramp (Figure 2). The vector plot for meter 5-1 shows a bimodal pattern with flood and ebb currents directly opposed, but much

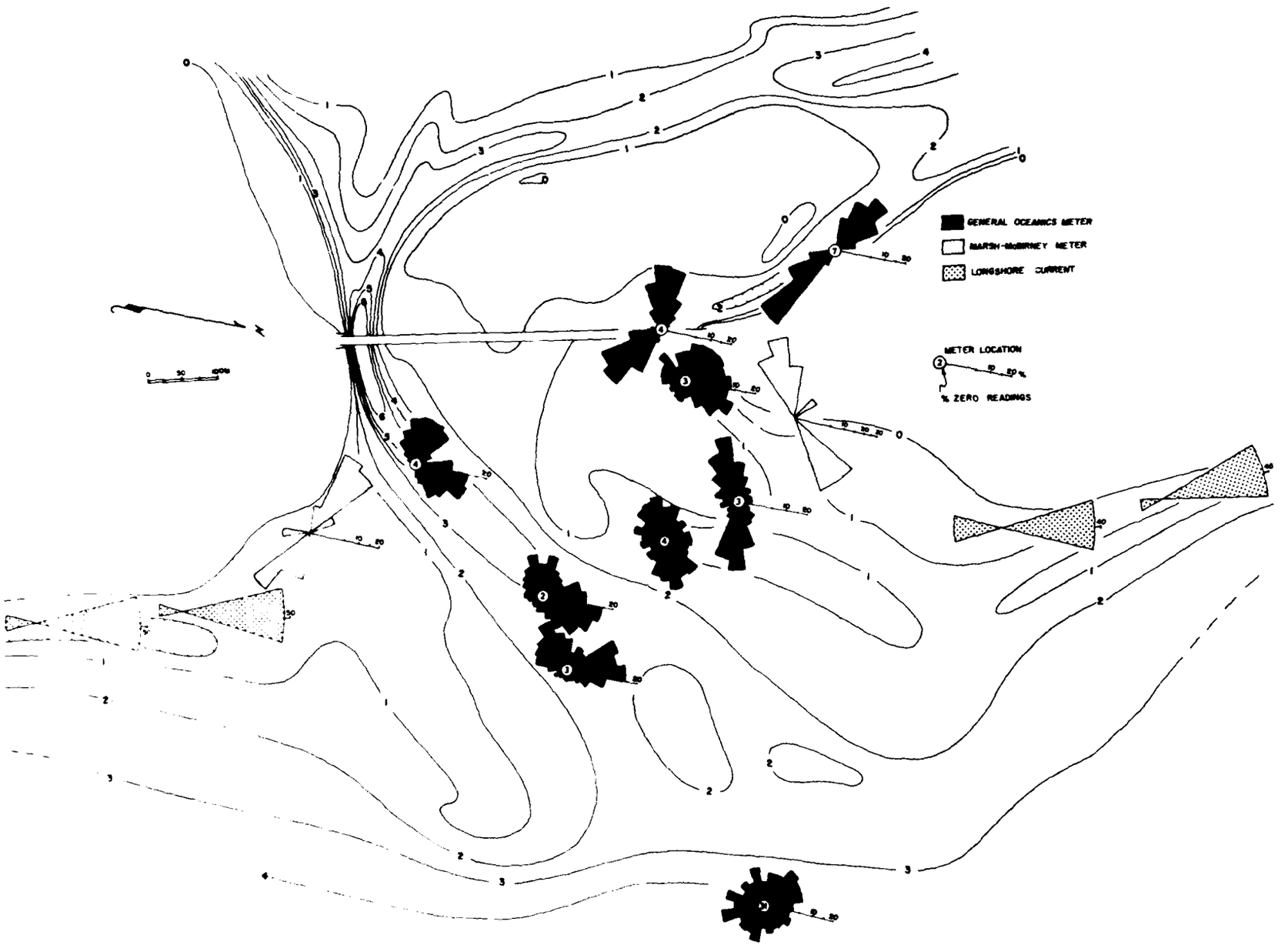

Figure 18. Rose diagrams showing current directions for all locations during summer 1978 study period.

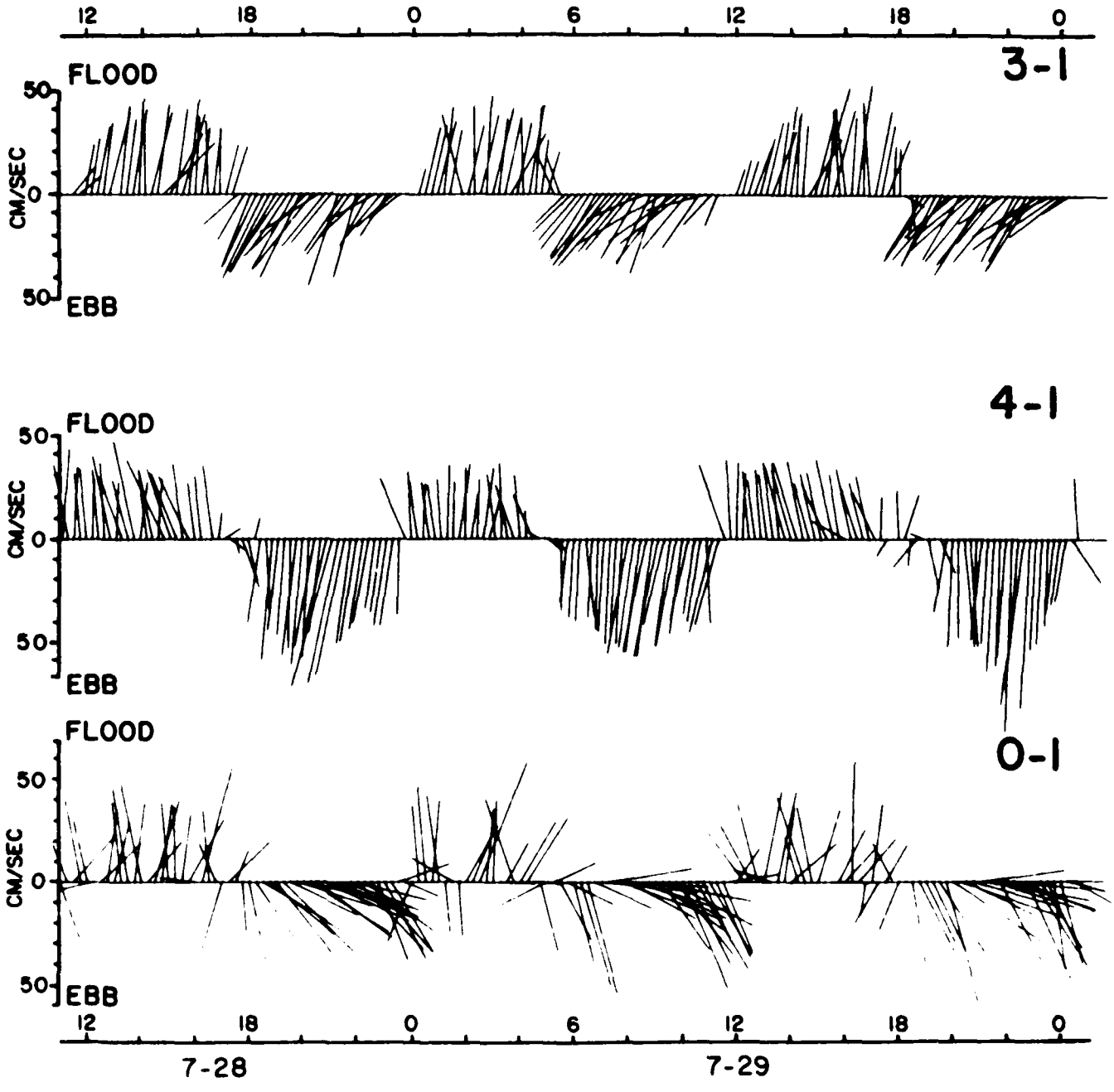

Figure 19. Vector diagrams for selected meter locations (see Figure 3) on July 28 and 29, 1978. Orientation of the horizontal axis is parallel with bridge over the inlet (N12W).

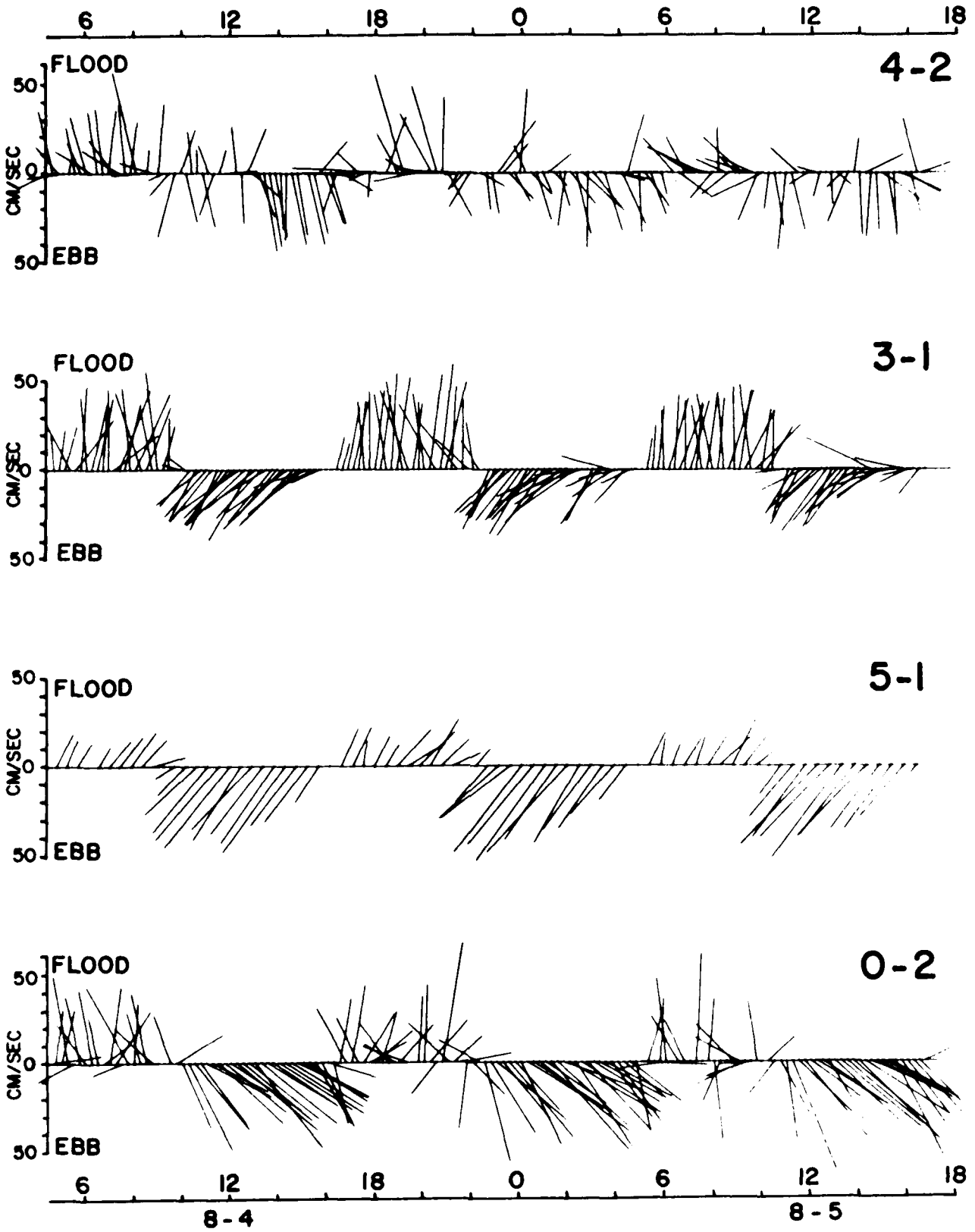

Figure 20. Vector diagrams for selected meter locations (see Figure 3) on August 4 and 5, 1978. Horizontal axis is parallel to bridge.

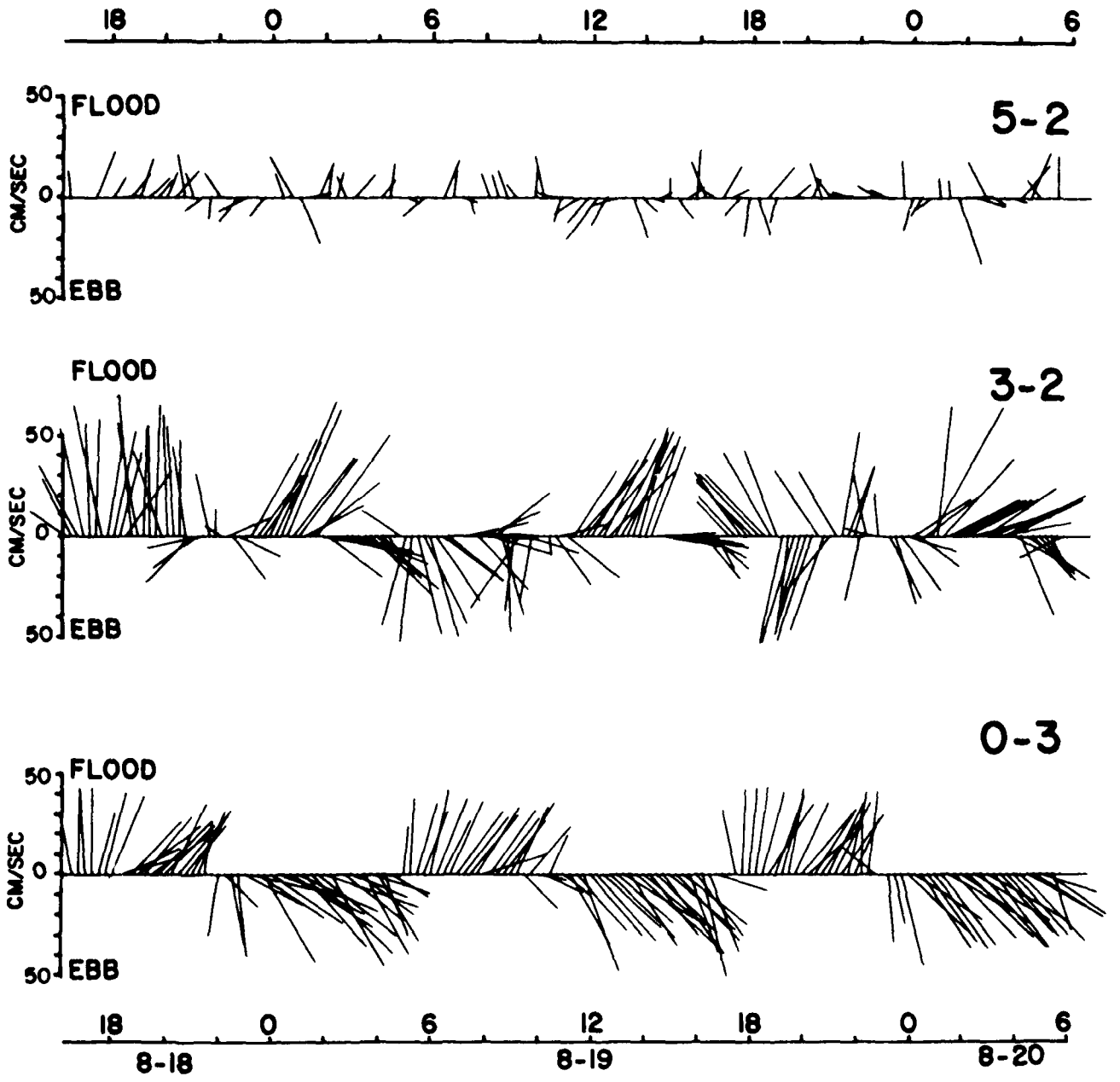

Figure 21. Vector diagrams for selected meter locations (see Figure 3) on August 18-20, 1978. Horizontal axis if parallel to bridge.

higher ebb current velocity. Meter 0-2 is located in the main ebb channel landward of meter 0-1. The flood portion of meter 0-1 still shows the strong influence of wave action, and the ebb portion has a higher velocity which also shifts in a clockwise direction.

The velocity vector plots for meters 5-2, 3-2 and 0-3 on August 18 to 20 are given in Figure 21. Meter 5-1 was located seaward of the terminal lobe (Figure 2). Although it is still possible to discern ebb and flood components, they are dominated by the wave surge. Meter 5-1 demonstrates that the ebb and flood currents have little influence beyond the terminal lobe. Meter 3-2 located in the north flood channel shows the influence of the adjacent shoal area. The ebb portion of the plot is split into 2 parts, one when the mid-channel shoal is submerged and a second when the shoal is exposed. The currents change direction almost 60° when the shoal area becomes exposed. A similar pattern is seen during the flood. Meter 0-3 is the most landward meter in the ebb channel. The meter shows the shift in current direction during the ebb, which was noted for meter 0-1 and 0-2. It also shows a shift in the flood pattern under the influence of longshore currents. When strong longshore currents are moving into the south flood channel, their effects are felt into the middle of the ebb channel.

Data from the moored current meters were also resolved into orthogonal components to estimate the flood and ebb components of the tide. The modal flood direction from the current rose (Figure 18) was used to plot the tide component with flood being a positive and the ebb negative (Figure 22). The residuals at right angles to the tide component are considered as the wave component because they are superimposed on the tides. For meter 5-1 in the channel adjacent to the ebb spit, the flood current velocity averages about 35 cm/s. The ebb current in the same channel reaches about 70 cm/s. The total current is plotted along the base of Figure 22 showing the larger ebb currents alternating with smaller flood currents. The location of the channel behind the bridge embankment accounts for the dominance of ebb currents. The ebb currents are directed to the southeast directly out the channel, but the flood currents do not reach maximum velocity in the protected channel.

The wave and tide components for meter 3-1 generate symmetrical tidal components (Figure 23). The ebb and flood portions of the tide component are equal to about 50 cm/s and the wave component varies from 20 to -40. Meter 3-1 was moored under the bridge near the north end of the north flood channel (Figure 2). The current rose for meter 3-1 (Figure 18) shows the difference in current directions for the ebb and flood currents. The flood current is flowing into the inlet across the flood ramp, but the ebb current is an extension of the current seen in the channel location for meter 5-1. The plot of total current for meter 3-1 shows the balance between ebb and flood current.

Meter 5-2, located beyond the terminal lobe, lacks a distinctive tidal component, but shows the influence of longshore current in the wave component (Figure 24). Meter 5-2 was located seaward of the terminal lobe and out of the effective influence of tidal currents. Near the end of the

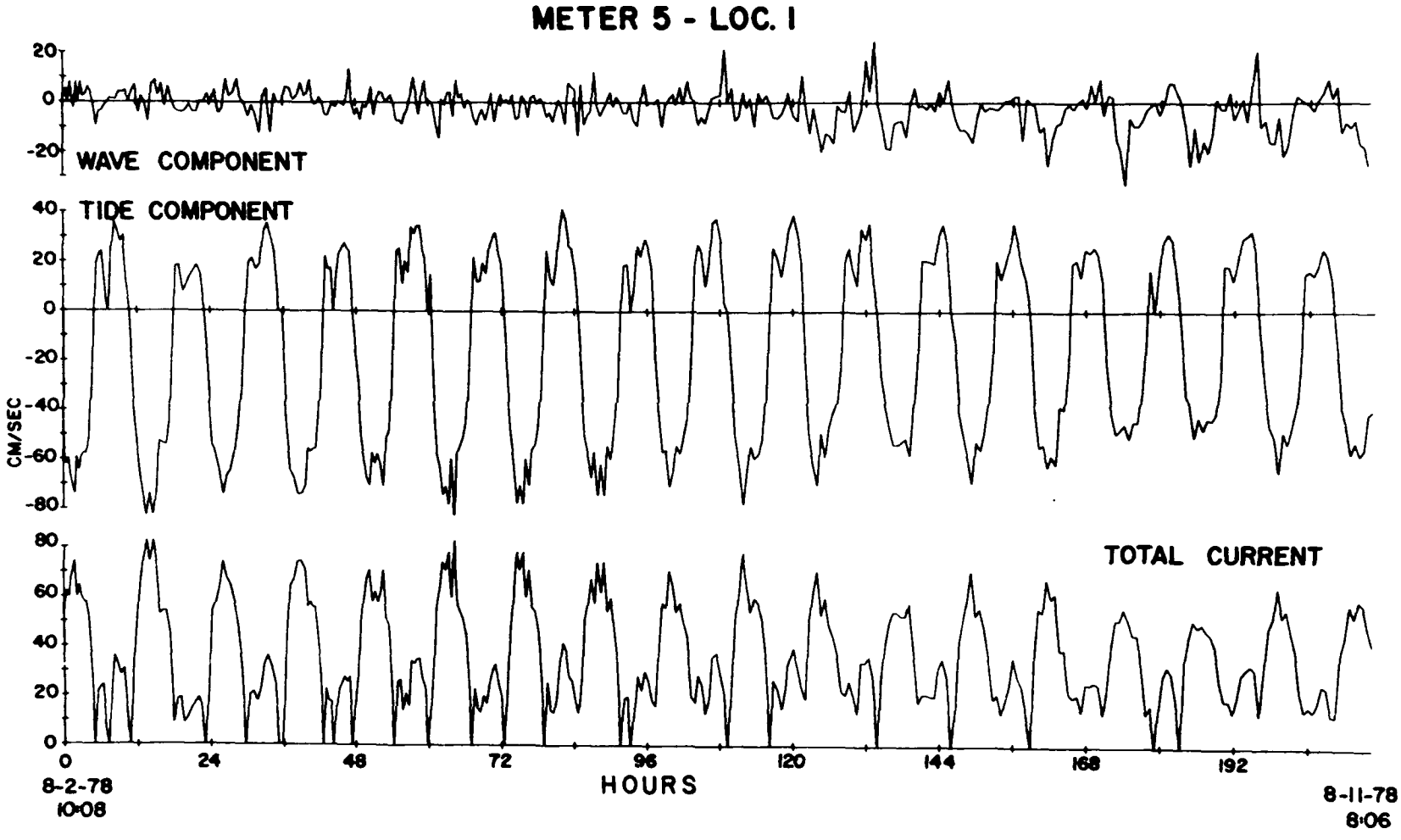

Figure 22. Current meter data at location 5-1 (see Figure 3) for the period of August 2-11, 1978. Note the strong ebb dominance of currents at this location and the small amount of variation attributed to wave action.

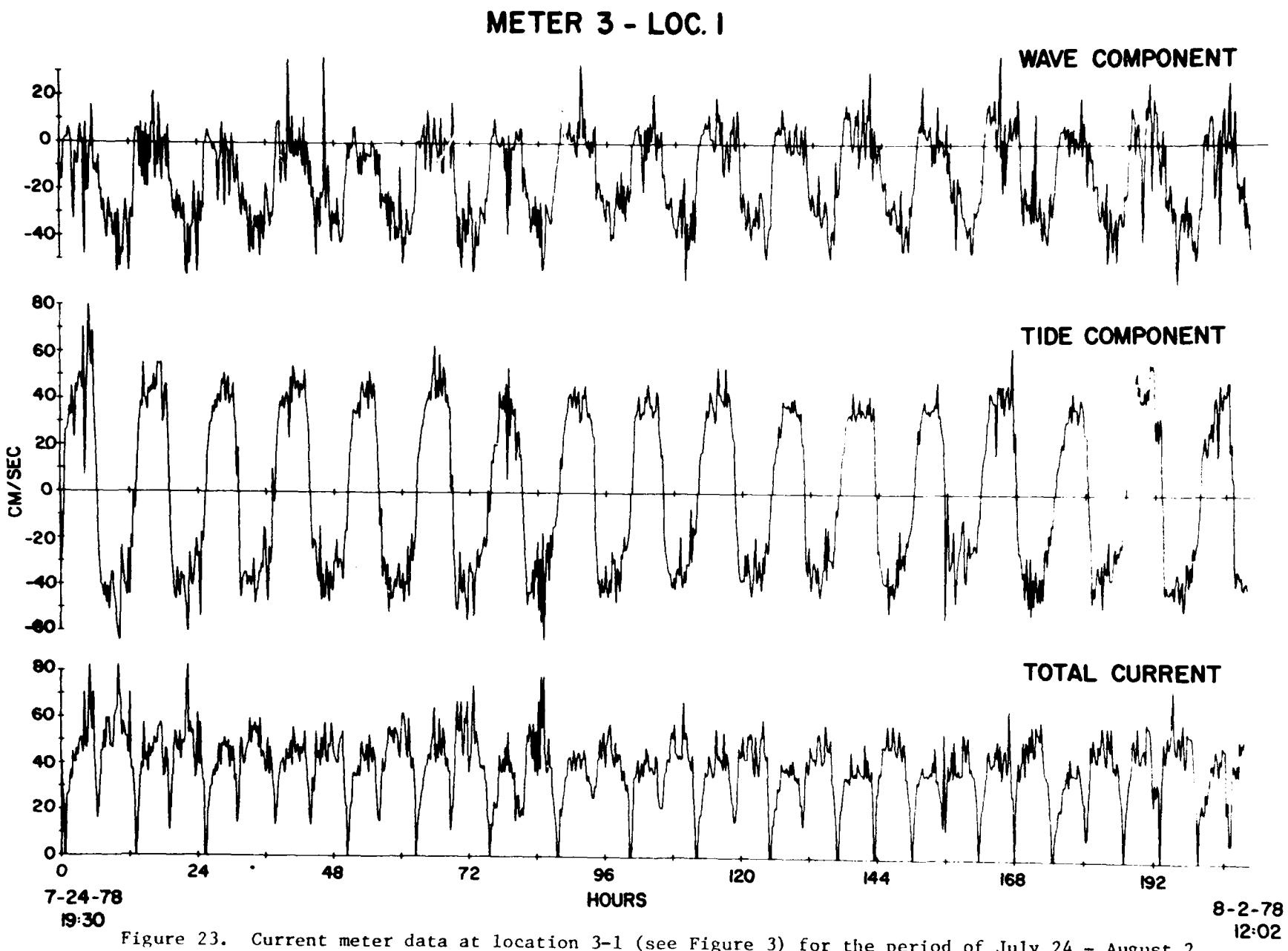

Figure 23. Current meter data at location 3-1 (see Figure 3) for the period of July 24 - August 2, 1978. Current speed is comparable during both flood and ebb stages, and these appear to be a significant component in the total variation.

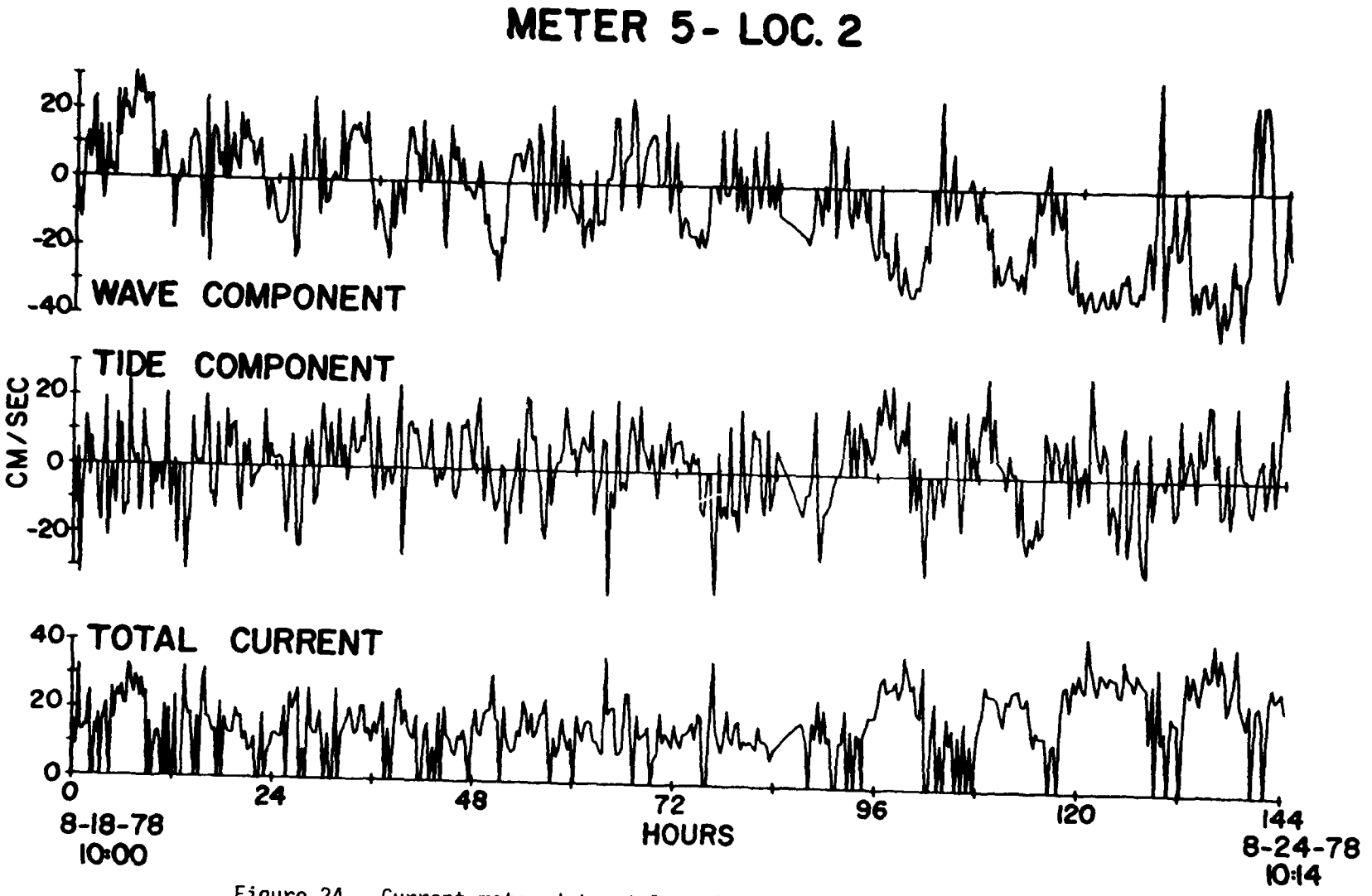

Figure 24. Current meter data at location 5-2 (see Figure 3) for the period of August 18-24, 1978. Note that current speeds are low and well-defined ebb and flood cycles are not present.

study, a southward flowing longshore current extended around the terminal lobe and induced a negative (southward) current to the wave component. The steady longshore component reached about 40 cm/s on August 23 (Figure 24).

Smoothed tidal curves

Smoothed tidal curves were computed and plotted for each meter to determine the average tidal velocity at twelve stages of the tide (Figure 25). The speed and direction data, taken at 15 minute intervals for the entire meter record were used to compute the daily average tidal curve for each meter. The compass rose diagrams (Figure 18) provided the dominant flood and ebb directions. The coefficients for the six major tidal harmonics (24.84, 12.42, 8.28, 6.21, 4.97 and 4.14 hours) were computed by Fourier analysis and plotted to produce the smoothed curves for ebb and flood. The curves plotted for meters 3-1, 5-1, 0-3, and 4-2 are composite curves with the flood portion of the curve taken from a Fourier analysis in the flood direction, and the ebb portion from a Fourier analysis in the ebb direction (Figure 25). Meter 3-1 has equal flood and ebb velocities, but meters 0-3 and 5-1 show ebb dominance. Meter 4-2 has a mixed pattern due to the effect of a shoal area which is submerged at mid flood.

The meter data taken in January 1977 (Figure 17) show a more symmetrical ebb and flood pattern than the 1978 data. In January 1977, the ebb channel extended to the north roughly parallel to the north shore of the inlet. Longshore currents were from the north during the entire study. The Fourier plots for the major lunar and solar tidal components parallel to the ebb channel show a flood dominance on the north side of the inlet (Locations A, B, and C in Figure 26). These three meter locations are under the strong influence of the southward flowing longshore current which is superimposed on the flood current (Figure 17). The meters located directly seaward of the main ebb channel (Meters D and E in Figure 26) are ebb dominated. The ebb current flows out the main ebb channel on the south margin of the inlet throat and splits into two segments by the large triangular bar (Figure 17). The north portion of the ebb flows past meter D and the south portion moves along the south shore past meter E. Therefore, the flood current moves into the inlet along the north beach being reinforced by the longshore current, and the ebb current moves out through the main ebb channel and splits into 2 portions on either side of the triangular shoal.

MODEL OF TIDAL CURRENTS

A descriptive model was developed to portray the average circulation pattern in Matanzas Inlet during 12 time segments of the tidal cycle. The objective of the model is to describe how the speed and direction of currents change as a function of time, topography and strength of the longshore current. The model is displayed as a series of streamline maps (Figures 27 and 28), velocity contour maps (Figures 29 and 30) and interpretive maps showing the influence of tides and longshore currents for

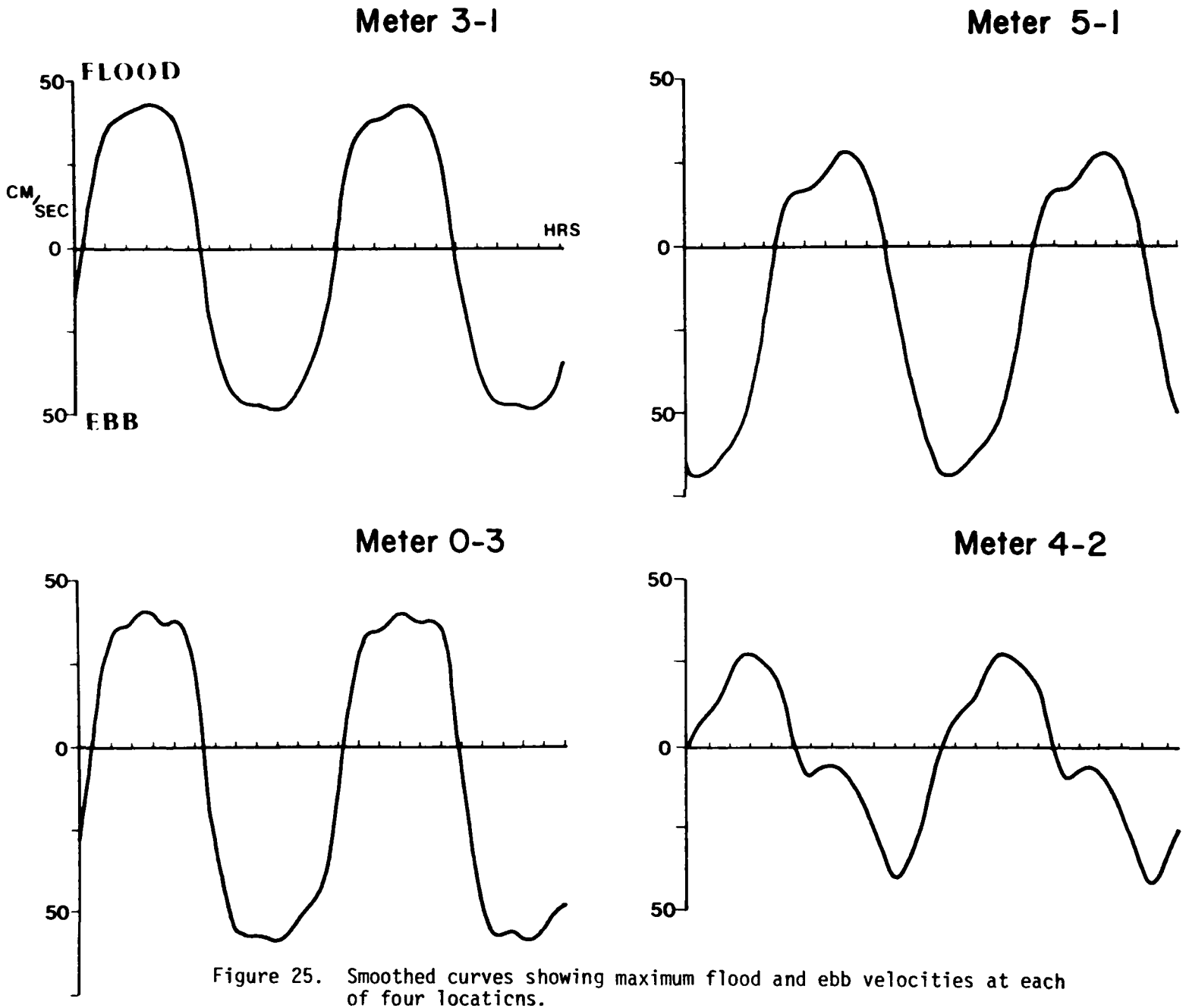

Figure 25. Smoothed curves showing maximum flood and ebb velocities at each of four locaticns.

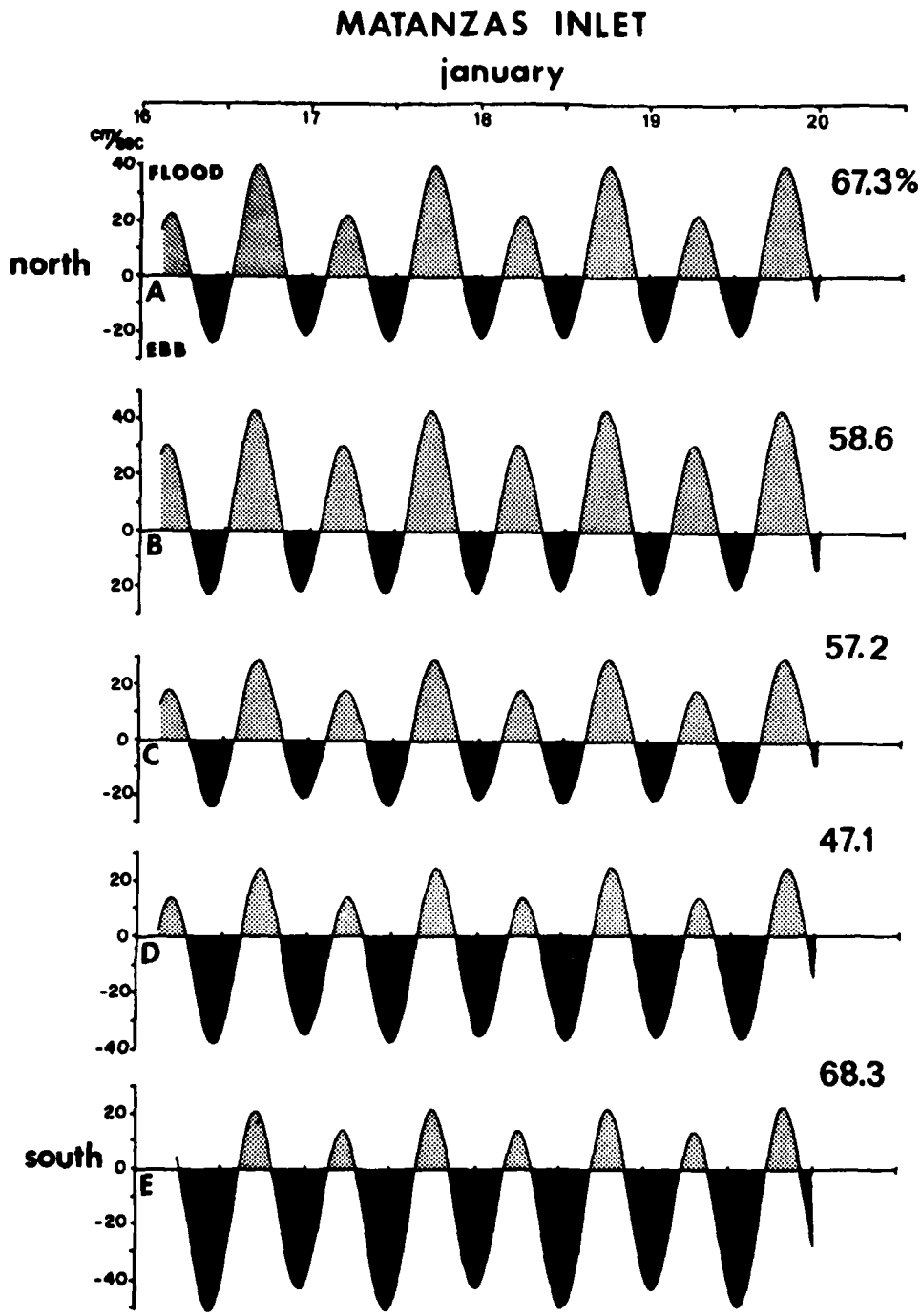

Figure 26. Smoothed Fourier curves for current meter data at five locations (see Figure 16). Note strong flood dominance at north side of inlet and ebb dominance on south side.

each time segment in the tidal cycle (Figures 31 and 32).

The first task in the construction of the model was to subdivide the tidal cycle into 12 segments; 6 for flood and 6 for ebb. Because the lengths of flood and ebb differ, the average lengths of flood and ebb were calculated, then divided into 6 equal segments. Based on the tide gauge data and predicted tides from July 27 through August 25, 1978, the average length of the flood stage was 6.06 hours, and average length of ebb was 6.36 hours. Therefore, the flood stage was divided into 1.01 hour segments, and the ebb was divided into segments with a duration of 1.06 hours.

The vector mean current speed and direction for each of the 12 segments was calculated at each moored meter location (Tables 2 and 3), for the Marsh-McBirney meter in the south flood channel (Table 4), and for the 4 beach sites (Table 4). For the 9 moored meter locations, the average speed and direction was computed within an 18 minute (0.3 hour) window bracketing each tidal segment. This window permitted a minimum of two data points for each interval.

The current speed and direction in the south flood channel and the longshore current speed at each of the beach sites are given in Table 4. The Marsh-McBirney meter was positioned 0.3 meters above the bottom to record two components of flow in the south flood channel. At low tide, and during segments 2, 11, and 12, before and after low tide, the sensing head of the meter was not submerged, and current speed is not available. The longshore current speed and direction at the beach sites were recorded 4 times each day at predicted low, mid-flood, high and mid-ebb tides. The average speed was computed for each observation period and a smooth curve was plotted through the observed values to interpolate a longshore current speed at each tidal segment.

Streamline and Contour Maps

A series of streamline maps showing the direction of the currents for each of the 12 time segments was plotted from the speed and direction data (Figures 27 and 28). The base map for each tide segment shows the extent of exposed intertidal sand bodies. The streamline maps of the 12 segments give a graphic representation of the changing current direction through time. A series of velocity contour maps was plotted on the same base as the streamline maps (Figures 29 and 30). The velocity contour maps are reproduced for the odd segments in the tidal cycle. The maps are individually discussed with the flood and ebb stages.

The model is for low energy conditions during the summer of 1978 when the longshore current flowed to the north. A similar model was constructed for the few days near the end of the study when the longshore current reversed to the south. The current pattern was modified by the longshore current and null lines occurred on opposite sides of the inlet. Because of limited time of south longshore currents, the model is not as precise, and the streamline and velocity contour maps are not reproduced. However, the current trends are incorporated in the generalized model showing the effects of different longshore currents.

Table 2. Average bottom current directions at the 12 tidal stages measured by moored tilt current meters.

	TIDE STAGE	Time	0-1	0-2	0-3	3-1	3-2	4-1	4-2	5-1	5-2
	Low	0	36.2	35.9	26.1	141.7	18.5	86.7	329.1	126.0	212.4
	2	1.01	310.5	250.3	32.0	274.0	205.1	257.0	235.5	296.5	273.6
F	3	2.02	267.5	263.8	242.0	269.3	193.4	245.7	200.1	293.3	342.3
L	4	3.03	280.4	268.4	284.6	263.8	241.1	243.4	227.0	295.1	200.9
O	5	4.04	271.6	262.4	283.4	266.4	292.9	233.6	218.2	312.1	217.8
O	6	5.05	282.9	255.4	293.5	267.2	260.1	230.1	196.8	309.6	196.4
D	High	6.06	284.9	261.7	275.4	261.9	306.3	235.4	206.0	333.5	198.0
	8	7.12	11.4	16.2	259.2	211.5	296.4	46.7	47.5	126.5	168.0
	9	8.18	19.5	8.4	17.1	120.2	340.9	77.7	30.2	134.7	170.0
E	10	9.24	6.1	13.2	16.0	128.3	316.6	80.7	31.9	136.4	147.4
B	11	10.30	7.2	9.1	14.7	134.2	323.7	88.2	55.1	131.4	93.4
B	12	11.36	24.2	3.4	10.7	139.5	353.7	88.3	60.5	130.8	45.4
	Low	12.42	36.2	35.9	26.1	146.7	18.5	87.6	329.1	126.0	213.4

Table 3. Average bottom current speeds during the 12 tidal stages measured by tilt current meters.

	TIDE STAGE	Time	0-1	0-2	0-3	3-1	3-2	4-1	4-2	5-1	5-2
	Low	0	45.4	44.0	44.1	29.4	38.5	39.9	16.1	26.8	5.8
	2	1.01	18.9	26.7	8.5	15.5	14.5	28.4	5.0	21.0	8.6
FLOOD	3	2.02	28.4	34.8	30.2	33.4	34.7	30.7	9.3	17.6	1.0
FLOOD	4	3.03	25.8	31.4	35.9	38.7	23.8	33.4	19.4	13.3	1.6
FLOOD	5	4.04	23.0	33.5	39.9	41.9	10.5	31.6	30.2	30.0	3.7
	6	5.05	22.3	29.1	38.1	44.7	13.0	26.0	20 9	29.9	5.1
	High	6.06	21.3	12.3	35.1	39.6	6.6	22.6	15.0	19.7	12.0
	8	7.12	11.5	22.1	14.8	5.4	2.8	11.3	9.2	17.3	17.9
	9	8.18	48.4	54.3	45.6	43.4	35.6	31.3	8.8	56.3	19.4
EBB	10	9.24	56.4	62.2	55.0	47.9	47.3	52.5	10.7	64.4	15.3
EBB	11	10.30	60.5	64.5	58.0	44.9	45.1	53.8	36.2	63.1	12.8
	12	11.36	56.7	59.8	51.5	44.8	44.9	52.9	36.4	51.6	1.7
	Low	12.42	45.4	44.0	44.1	29.4	38.5	39.9	16.1	26.8	5.8

Table 4. Average speed and direction when water was flowing through the south flood channel and average longshore current velocities to the north at locations R, O, B, and E.

TIDE STAGE	South Flood Channel SP	DIR	Longshore current speed (cm/sec) R	O	B	E
Low	--	---	27.6	21.4	33.5	30.6
2	--	---	27.9	30.7	25.0	25.9
3	76.5	303	28.1	40.6	16.2	20.8
4	76.5	299	28.3	50.4	7.2	15.8
5	71.5	298	31.6	53.5	5.2	16.3
6	69.5	296	35.0	56.2	2.8	16.8
High	53	296	37.9	59.1	0.4	17.3
8	2	187	34.5	47.5	6.5	18.7
9	96	107	31.0	35.7	13.3	20.1
10	139	124	27.0	22.8	20.7	21.6
11	--	---	27.3	22.4	24.7	24.6
12	--	---	27.5	22.0	29.4	28.0
Low	--	---	27.6	21.4	33.5	30.6

Flood stage

The current pattern during flood stage is shown on the streamline map (Figure 27). At low tide (Time segment 1) the currents are flowing out of the inlet and to the north. The swash bars flanking the ebb channel are exposed above sea level and the current is restricted to the deeper portions of the channel. The highest velocity is about 80 cm/s where the channel is constricted under the bridge, but seaward of the bridge, the speed drops off to about 45 cm/s (Table 2).

At time segment 2 about 1 hour after low tide, the currents in the inlet are shifting from ebb to flood. Two null lines are present on the map for segment 2 which indicate the lines along which the currents are changing direction. The null line passing from the south shore of the inlet across to a middle shoal started near the terminal bar and moved progressively landward into the inlet. The null line marks the convergence of waning ebb currents and developing flood current and takes about 40 minutes to move into the inlet. The null line at the north side of the inlet forms at the divergence between ebb currents move off to the north and the ebb current head into the inlet. The longshore null line maintains its approximate position throughout the rest of the flood stage. The null line is evidenced by a shoal area on the bottom contour map (Figure 5).

Segments 3 through 7 show the full development of the flood portion of the tidal cycle. As the flood progresses, the channel margin bars are progressively submerged and the longshore current plays a significant role. Near low tide, the incoming flood currents follow the main channel, but as longshore currents spill over the south marginal bars, the current direction shifts over from the south. The highest flood current velocities are encountered in the flood channels on the north and south sides of the inlet. In the south channel, the speed reaches 76 cm/s and in the north channel under the bridge, maximum speed is 105 cm/s. In the main channel, the bottom currents reach about 40 cm/s while surface currents under the bridge exceed 80 cm/s. The increasing influence of the longshore current on the flood currents can be seen in the velocity contour map along the south side of the inlet (Figure 27). The area of maximum current velocity shifts from the center of the channel to the south margin hugging the south flood channel.

Ebb stage

The ebb stage which extends from high through low tide marks the maximum current velocities in the main channel. At high tide, time segment 7, the ebb currents are still flowing into the inlet. At segment 8, about an hour after high tide a null line bisects the inlet with flood currents continuing to enter along the south, while ebb currents are flowing out along the north margin. At segment 9, the ebb current pattern becomes fully developed with a null line along the south margin of the inlet. During the ebb, the longshore currents converge with the ebb currents and flow out to sea along the null line. This is directly opposite to the

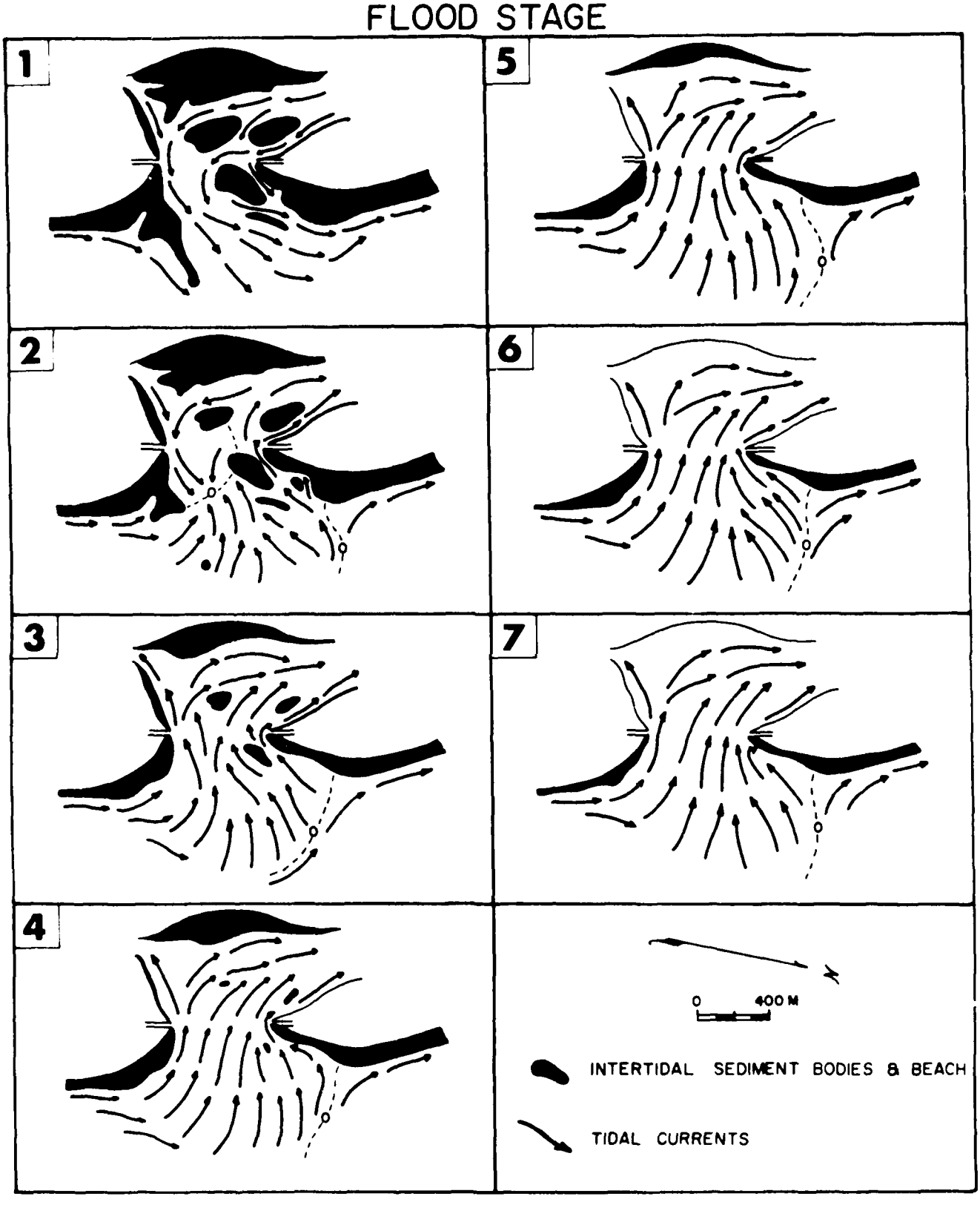

Figure 27. Circulation patterns during flood tidal cycle. Zero contour represents a null line.

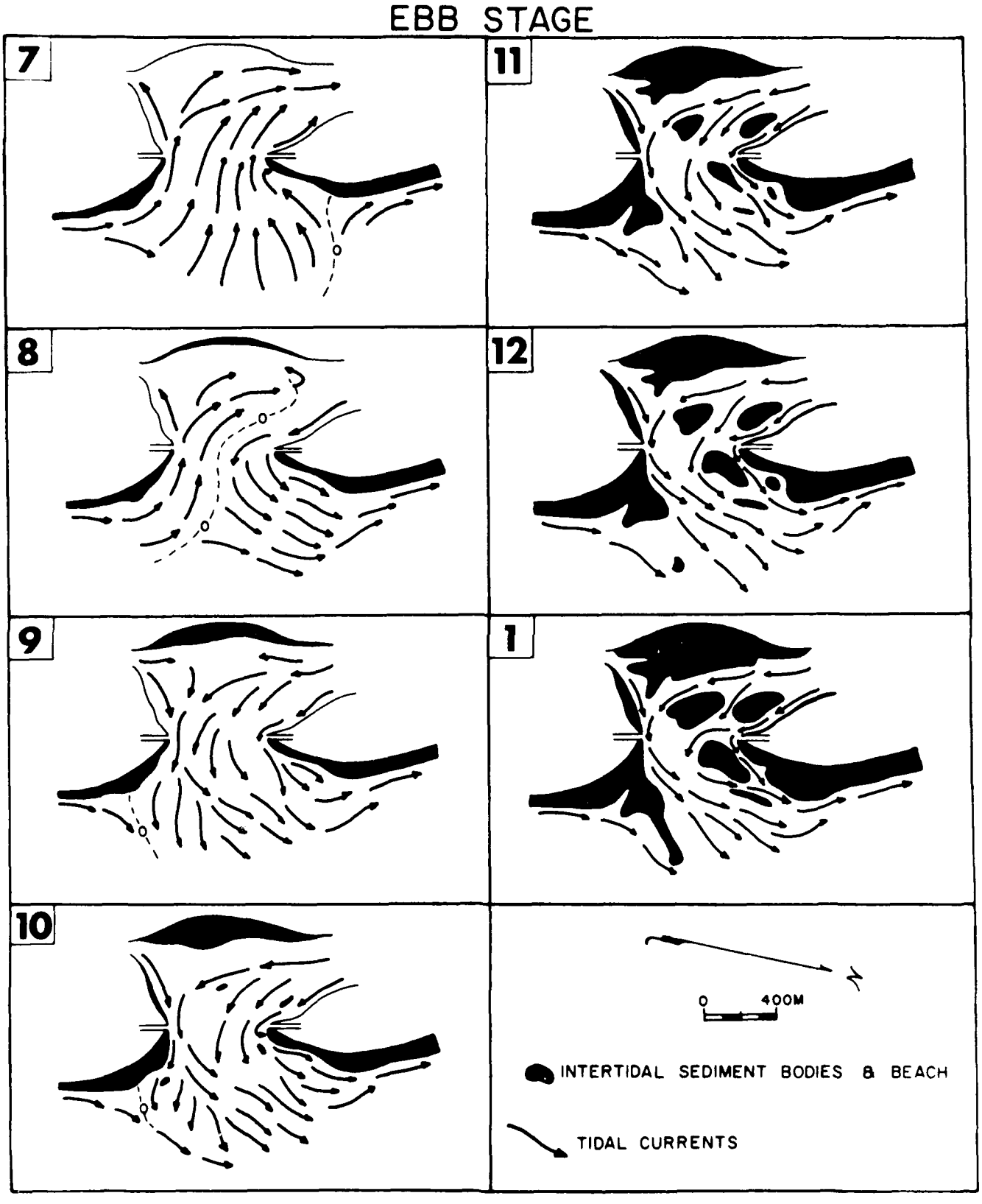

Figure 28. Circulation patterns during ebb tidal cycle. Zero contour represents a null line.

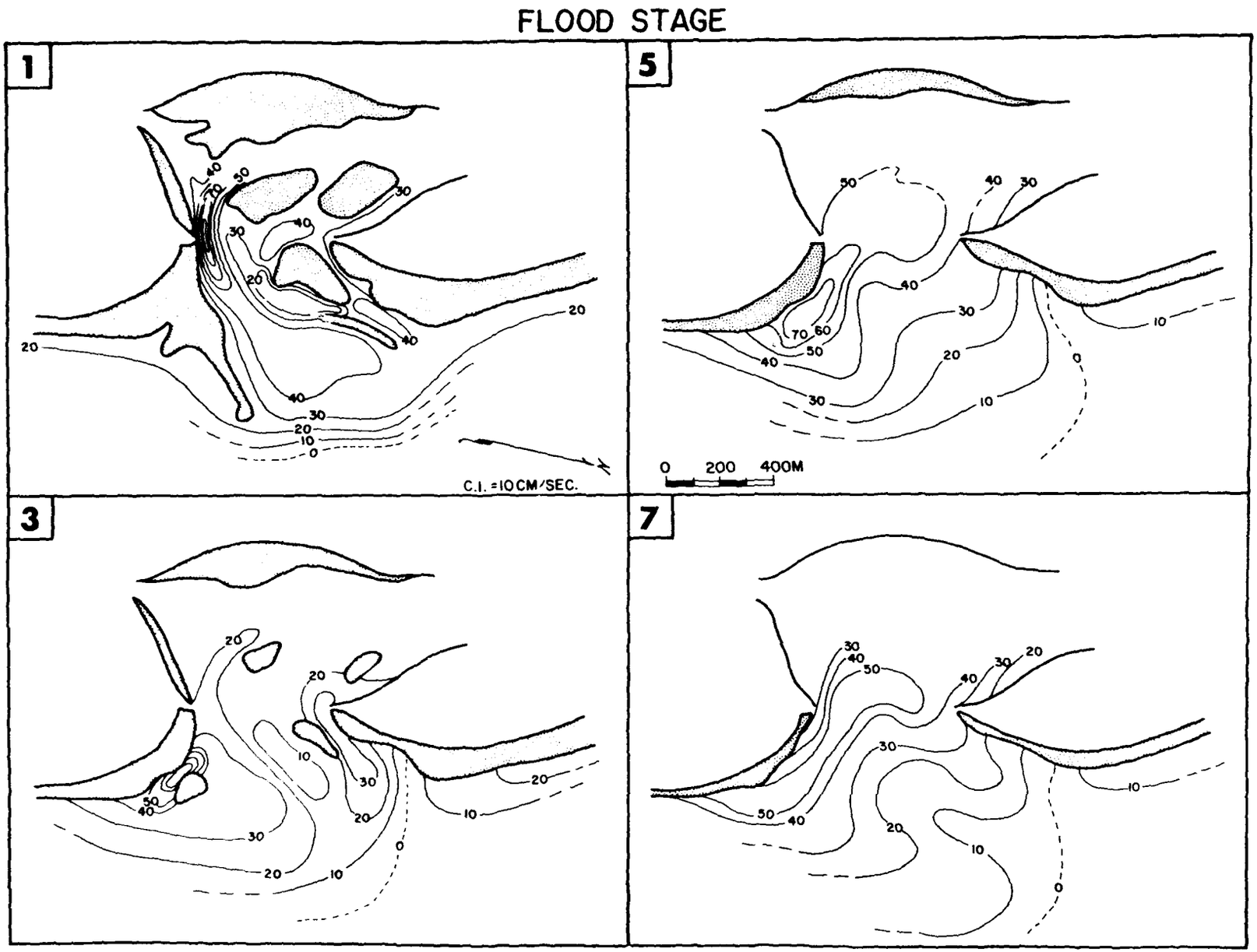

Figure 29. Contour map of current speeds during flood stage.

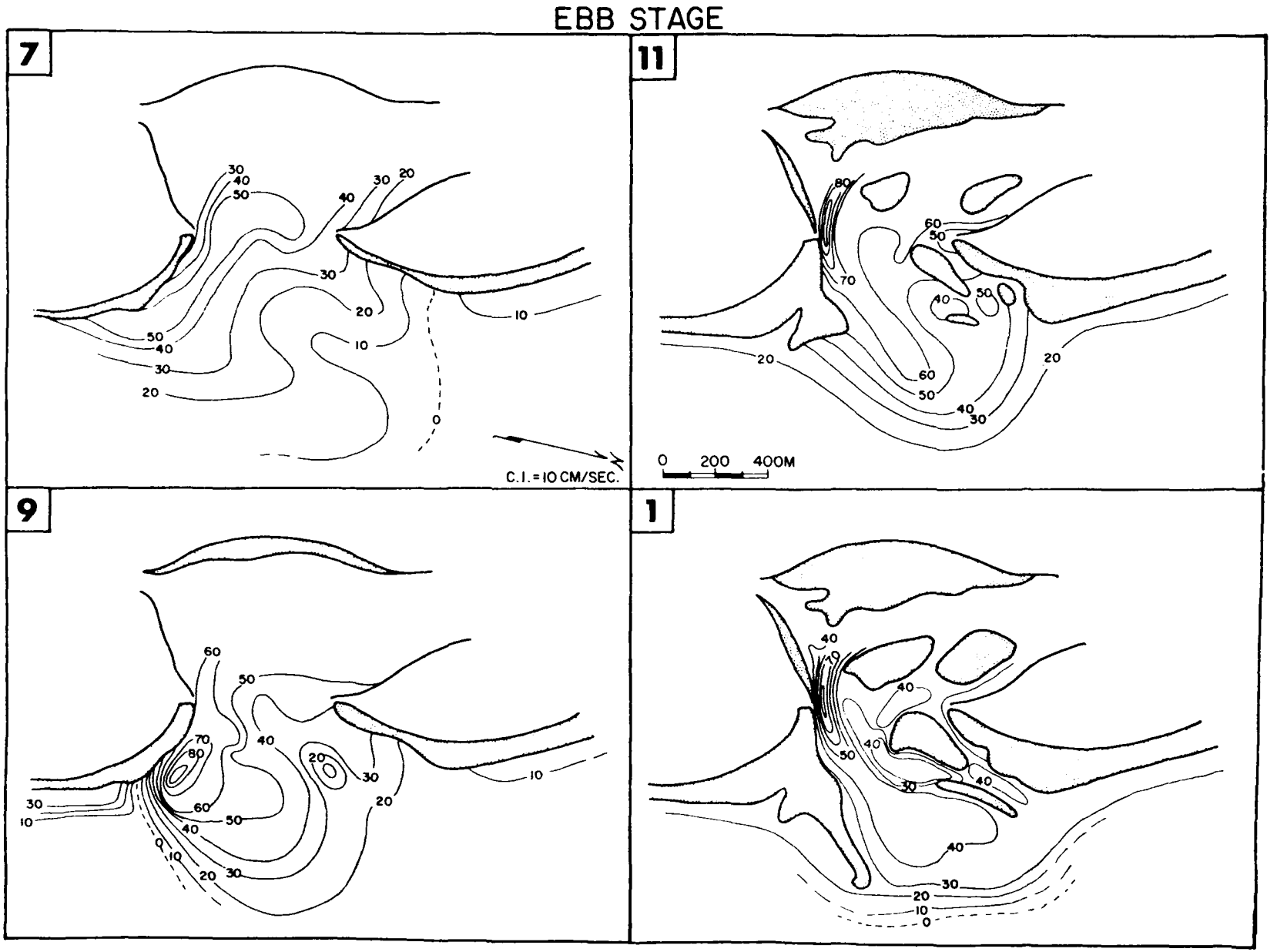

Figure 30. Contour map of current speeds during ebb stage.

conditions during the flood stage when the flood and longshore currents diverge along the null line at the north side of the inlet. As the ebb stage progresses, the intertidal sand bodies once again emerge above sea level and the south margin linear bar appears along the null line. The ebb currents flow to the northeast and merge with the northward flowing longshore current.

Generalized Flow Maps

The model for flood and ebb stages is summarized in the generalized maps for north and south longshore currents. For each time segment, the outlined arrows indicate the tidal and longshore currents when the longshore current is to the south, and the stippled arrows indicate the currents when the longshore current is to the north (Figures 30 and 31). The null lines are dashed when the longshore current is to the south, and solid when the current is to the north.

During the flood stage, the null line is generally on the south side of the inlet when longshore is to the north, and on the north side of the inlet when the current is to the south (Figure 31). The incoming current diverges at the null line with a portion of the current heading into the inlet and a portion heading along the beach. A complicated pattern of currents and null lines develops when the currents change from ebb to flood. In essence, the null line migrates into the throat of the inlet from the terminal lobe, then shifts to the downcurrent side of the inlet for the remainder of the flood stage (Figure 31).

The generalized maps for the 6 segments of the ebb stage start out with a flood tide pattern (Figure 32). At time segment 8, the null line shifts from one side of the inlet to the other. For segments 9 through 12, the main flow is out the ebb channel. A null line is formed at the upcurrent end where the ebb current and longshore currents converge. At the downcurrent side of the inlet, the longshore current forms a shear with ebb current. The ebb current and downcurrent part of the longshore current are separated by shoal areas except near high tide, so the shearing action is only evident early in the ebb stage. The generalized action of tidal currents, longshore currents and direction of wave approach is given in Figure 33. The dashed line marks the outline of the terminal lobe.

In summary, the distinctive features for the ebb and flood stages are the position of the null line and its relationship to the longshore current. During flood, the null line is located at the downcurrent side of the inlet and flood current and longshore current diverge along the null line. During ebb, the null line is located on the upcurrent side of the inlet and the ebb current converges with the longshore current along the null line. When the longshore current shifts from north to south, the null line changes position from one side of the inlet to the other. The shoals on the margin of the inlet form at the position of the null lines with the dominant shoal formed during the ebb stage. The terminal lobe marks the seaward extent of the tidal currents and merges with the marginal shoals on each side of the inlet.

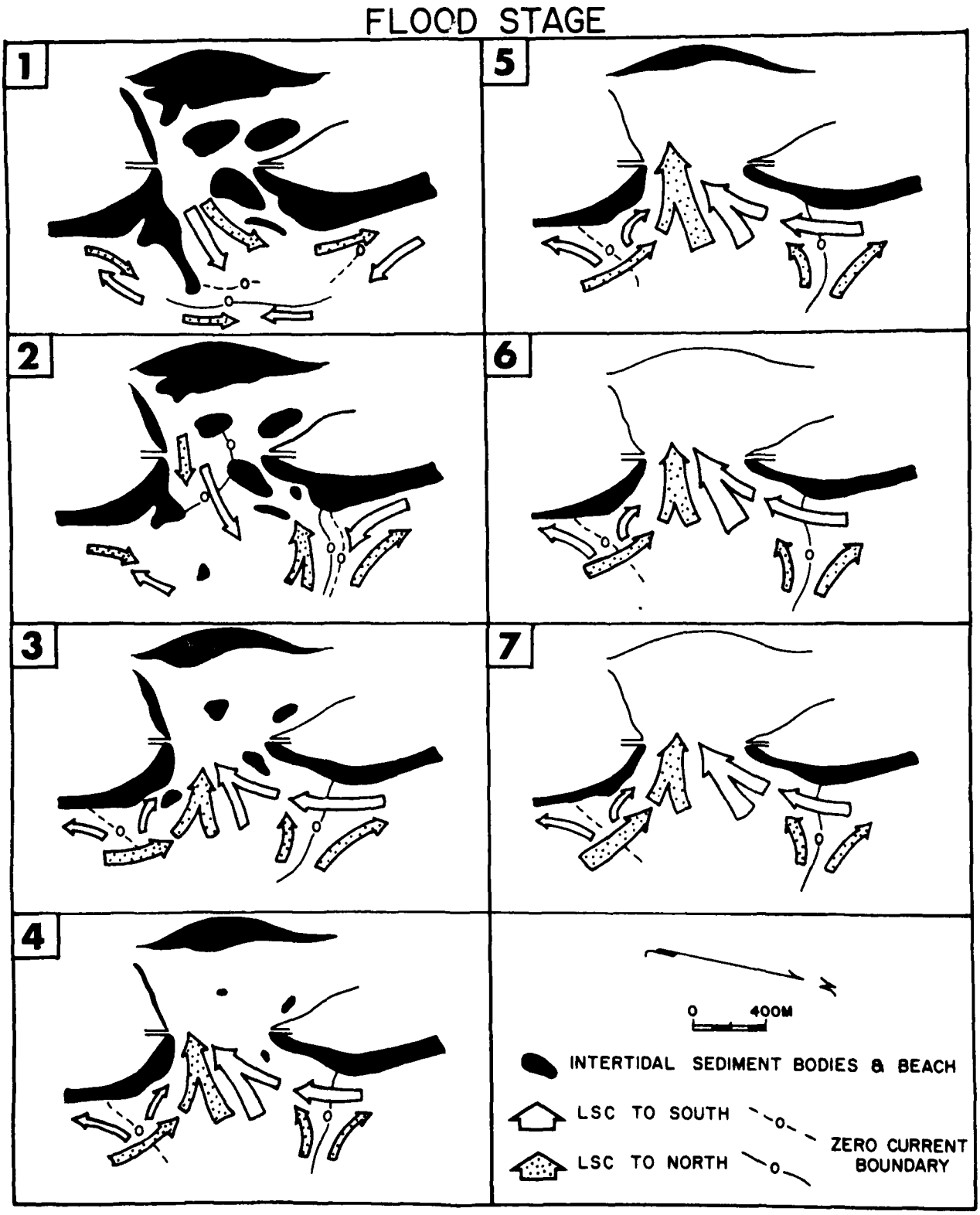

Figure 31. Generalized flow map for currents during flood stage. Zero contour represents null line.

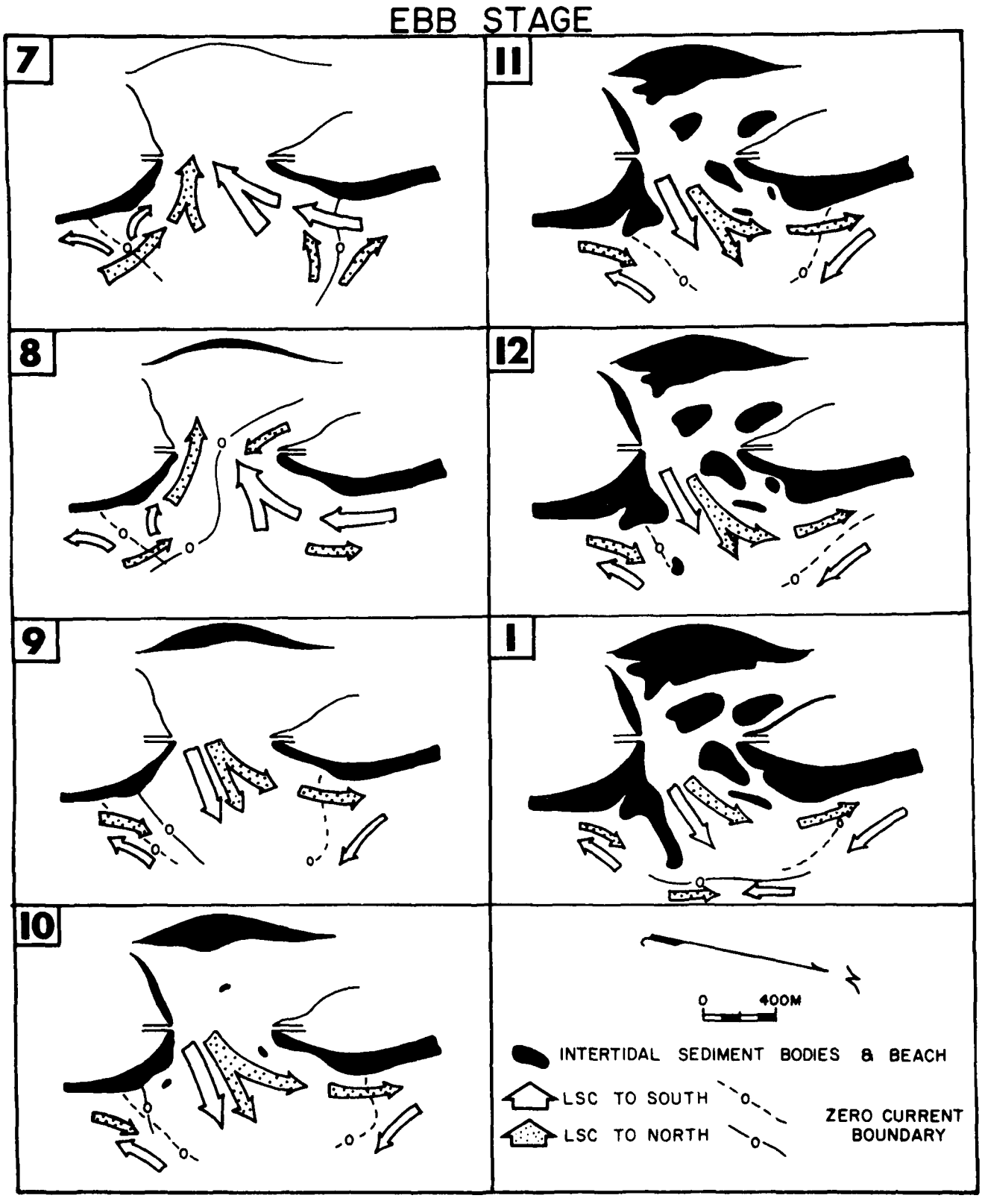

Figure 32. Generalized flow map for currents during ebb stage. Zero contour represents null line.

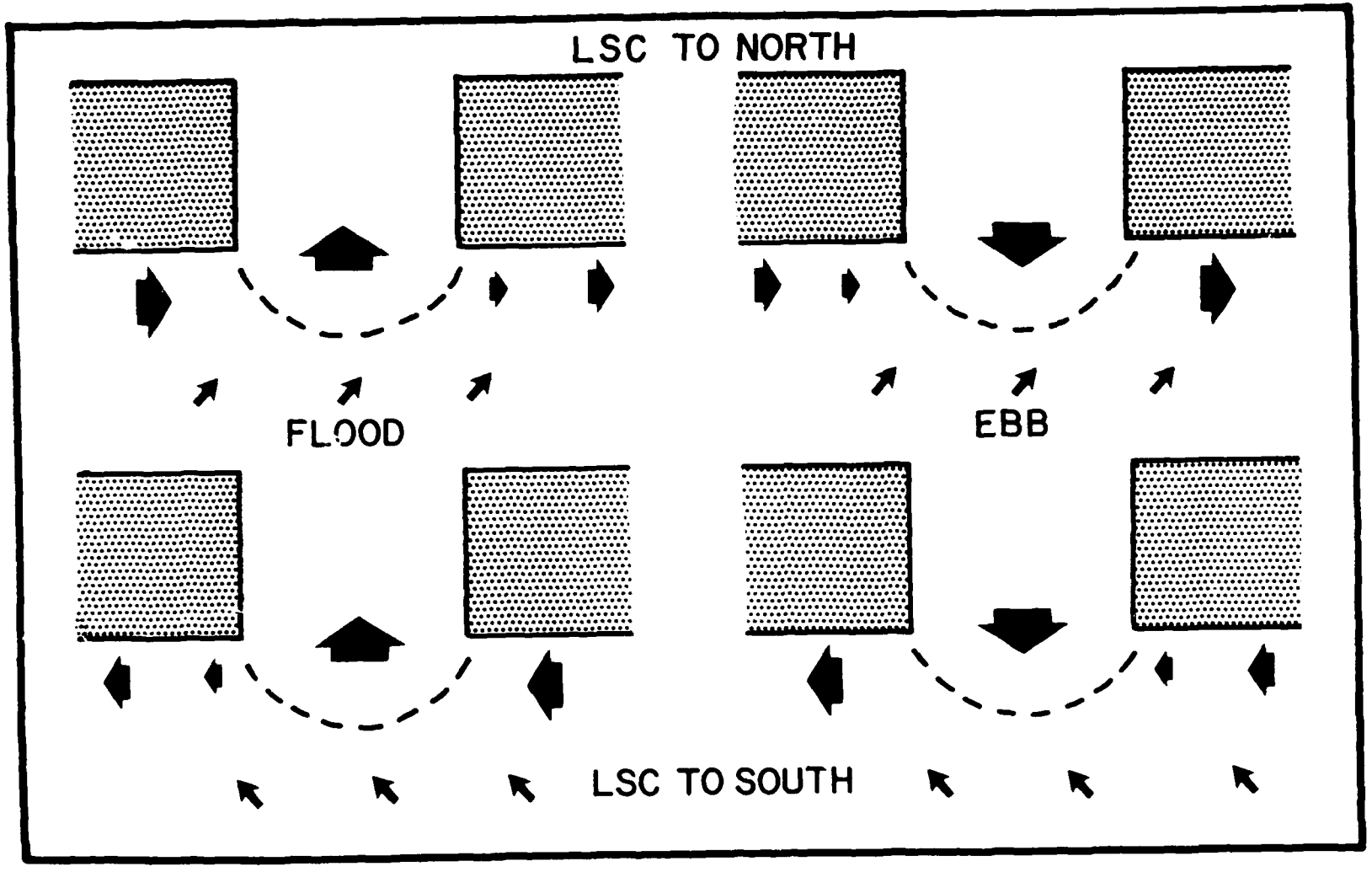

Figure 33. General process model for inlet-beach transition for ebb and flood stages during both north and south flowing longshore current.

SUMMARY

The present study represents the first attempt to characterize the beach-inlet transition zone of natural tidal inlets. Although this is a very dynamic environment there are patterns which can be resolved and thereby permit construction of general models. The following statements summarize the data collected during the feasibility study in January, 1977 and the extended field study in the summer of 1978:

1) Weather patterns in the Matanzas Inlet area are seasonal and thereby create a seasonality to longshore currents. During summer longshore currents are primarily south to north whereas they are north to south during the winter.

2) Waves in the inlet area are largely affected by water depth and therefore tidal stage. There is also some reinforcement of wave size during flood tides and dampening of waves by ebb currents.

3) Longshore currents respond in a predictable fashion to flooding and ebbing tidal currents.

4) The extent of influence of tidal currents is limited to a radius of only a few hundred meters from the inlet mouth.

5) Tidal currents may display markedly different flood and ebb directions at a given location than the expected opposite orientation. This is due primarily to the overall inlet shape and to the influence of channels on tidal current direction.

6) Morphology of Matanzas Inlet changed markedly between January, 1977 and the summer of 1978. The main channel was deflected to the north in 1977 but was essentially central to the inlet in 1978. In addition, sediment from the flood delta moved seaward during that period. These changes are in response to changes effected by closing the storm cut on Rattlesnake Island. Present morphology appears to represent equilibrium conditions and is similar to that which prevailed prior to the storm generated breach of the island.

7) Data available permit the development of a dynamic model which shows circulation patterns for each of 12 stages in the tidal cycle. Although this model is based on only one study it has potential for general application if supplemented by additional empirical data.

REFERENCES CITED

Boothroyd, J.C., 1978, Mesotidal inlets and estuaries, in Davis, R.A. (ed.), Coastal Sedimentary Environments, Springer-Verlag, Inc., New York, p. 287-360.

Brunson, T.Q., 1972, Sedimentological study of Matanzas Inlet, Florida and adjacent areas. M.S. Thesis, Univ. of Florida, 103 p.

Bruun, Per, 1968, Tidal Inlets and Littoral Drift. H. Skipnes Offsettrykker, Trondheim, Norway, 193 p.

Bruun, Per and Gerritsen, F., 1961, Natural bypassing of sand at coastal inlets and passes. Trans. ASCE, v. 126, Part IV, p. 823-854.

Davies, J.L., 1964, A morphogenic approach to world shorelines. Zeit. Geomorph., v. 8, p. 27-42.

Finley, R.C., 1975, Morphologic development and dynamic processes at a barrier island inlet, North Inlet, S.C. in Cronin, L.E. (Ed.), Estuarine Research, v. 2, Geology and Engineering, Academic Press, New York, p. 277-292.

Finley, R.C., 1976, Hydraulics and dynamics of North Inlet, S.C., 1974-75. GITI Report 10, U.S. Army Coastal Engineering Research Center, 188 p.

FitzGerald, D.M., Nummedal, D., and Kana, T.W., 1976, Sand circulation at Price Inlet, South Carolina, Proc. 15th Conf. on Coastal Engr., Honolulu, p. 1868-1880.

Fox, W.T. and Davis, R.A., 1963, Simulation model for storm cycles and beach erosion on Lake Michigan, Geol. Soc. Amer. Bull., v. 84, p. 1769-1790.

Fox, W.T. and Davis, R.S., 1976, Final report, comparison of computer simulation models with field data from nearshore environments. ONR Tech. Rept. No. 15, Contr. #388-092, Williams College, 54 p.

Fox, W.T. and Davis, R.A., 1979, Computer model of wind, waves and longshore currents during a coastal storm. Math. Geol., v. 11, p. 143-164.

Gallivan, L.B. and Davis, R.A., 1980, Sediment transport in a microtidal estuary: Matanzas River, Florida (U.S.A.) Marine Geology, v. 33, (In press).

Hayes, M.O., 1975, Morphology of sand accumulations in estuaries. in Cronin, L.E. (ed.), Estuarine Research, v. 2, Academic Press, New York, p. 3-22.

Hayes, M.O., Owens, E.H., Hubbard, D.K. and Abele, R.W., 1973, the investigation of form and processes in the coastal zone in Coates, D.R., (ed.), Coastal Geomorphology, Publ. in Geomorph., Binghamton, N.Y., p. 11-41.

Jonsson, I.G., Skougaard, C., and Wang, J.D., 1971, Interaction between waves and currents. Proc. 12th Coastal Engr. Conf., Washington, D.C., p. 489-507.

Lee, D.J., 1980, Sediments and bedforms at Matanzas Inlet, Florida. M.S. thesis, Univ. South Florida (In prep.)

Longuet-Higgins, M.S. and Stewart, R.W., 1960, Changes in the form of short gravity waves on steady uniform currents. Jour. Fluid Mech., v. 10, p. 529-549.

Mehta, A.J., 1978, Bed friction Characteristics of three tidal entrances. Coastal Engineering, v. 2, p. 69-83.

Mehta, A.J. and Jones, C.P., 1977, Matanzas Inlet. Glossary of Inlets Report #5. Florida Sea Grant Program, Rept. No. 21, 79 p.

NOAA, 1978, Tide tables, east coast of North and South America, U.S. Dept. of Commerce, National Oceanic and Atmospheric Administration.

Peregrine, D.H., 1976, Interaction of water waves and currents in Yih, C-S. (ed.), Adv. in App. Mechanics, Academic Press, Inc., New York, p. 9-117.

Phillips, O.M., 1966, The Dynamics of the Upper Ocean. Cambridge University Press, Cambridge, England.

Ritter, J.R., 1972, Sediment transport in a tidal inlet. Proc. 15th Conf. Coastal Engr., Vancouver, B.C., Ch. 44.

Seyferth, E.S., 1979, A new approach to the study of bed friction through computer models of flood channels. Senior thesis, Williams College, Williamstown, Mass., 208 p.

Sheridan, S.W., 1979, Eulerian and Lagrangian methods of collection and analysis of current data. Senior thesis, Williams College, Williamstown, Mass., 97 p.

Sonu, C.J., 1969, Collective movement of sediment in littoral environment, Proc. 11th Conf. Coastal Engr., London, p. 373-400.

Whitman, G.B., 1962, Mass, momentum and energy flux in water waves, Jour. Fluid Mech., v. 12, p. 135-147.

BASIC DISTRIBUTION LIST

Office of Naval Research — 12 copies
Coastal Sciences Program
Code 462
Arlington, Virginia 22217

Defense Documentation Center — 12 copies
Cameron Station
Alexandria, Virginia 22314

Director, Naval Research Laboratory — 6 copies
ATTN: Technical Information Officer
Washington, D. C. 20375

Director
Office of Naval Research Branch Office
1030 East Green Street
Pasadena, California 91101

Commanding Officer
Office of Naval Research Eastern/Central
Regional Office
Building 114, Section D
666 Summer Street
Boston, Massachusetts 02210

Office of Naval Research
Code 480
National Space Technology Laboratories
Bay St. Louis, Mississippi 39529

Director, Naval Research Laboratory
ATTN: Library, Code 2628
Washington, D. C. 20375

Commander
Naval Oceanographic Office
ATTN: Library, Code 1600
NSTL Station, MS 39529

Chief of Naval Operations
OP 987J
Department of the Navy
Washington, D. C. 20350

Defense Intelligence Agency
Central Reference Division
Code RDS-3
Washington, D. C. 20301

Director
Coastal Engineering Research Center
U.S. Army Corps of Engineers
Kingman Building
Fort Belvoir, Virginia 22060

National Oceanographic Data Center (D764)
Environmental Data Services
NOAA
Washington, D. C. 20235

Central Intelligence Agency
ATTN: OCR/DD-Publications
Washington, D. C. 20505

Coastal Studies Institute
Louisiana State University
Baton Rouge, Louisiana 70803

Dr. Douglas L. Inman
University of California A-009
Shore Processes Laboratory
La Jolla, California 92093

Dr. Robert Dolan
Department of Environmental Sciences
University of Virginia
Charlottesville, Virginia 22903

Dr. Benno M. Brenninkmeyer, SJ
Department of Geology and Geophysics
Boston College
Chestnut Hill, Massachusetts 02167

Dr. Choule J. Sonu
Tekmarine, Inc.
41 West Santa Clare St.
Arcadia, California 91106

Dr. Hsiang Wang
Department of Civil Engineering
Dupont Hall
University of Delaware
Newark, Delaware 19711

Dr. John T. Kuo
Henry Krumb School of Mines
Seely W. Mudd Building
Columbia University
New York, New York 10027

Dr. Edward B. Thornton
Department of Oceanography
Naval Postgraduate School
Monterey, California 93940

Dr. Richard A. Davis, Jr.
Department of Geology
University of South Florida
Tampa, Florida 33620

Dr. William T. Fox
Department of Geology
Williams College
Williamstown, Massachusetts 01267

Dr. William L. Wood
Department of Geosciences
Purdue University
Lafayette, Indiana 47907

Dr. J. Ernest Breeding, Jr.
Florida Institute of Technology
Department of Oceanography
Melbourne, Florida 32901

Dr. John B. Southard
Department of Earth & Planetary Sciences
Massachusetts Institute of Technology
Cambridge, Massachusetts 01239

Dr. John C. Kraft
Department of Geology
University of Delaware
Newark, Delaware 19711

Dr. Dag Nummedal
Department of Geology
Louisiana State University
Baton Rouge, Louisiana 70803

Dr. John D. Milliman
Department of Geology and Geophysics
Woods Hole Oceanographic Institute
Woods Hole, Massachusetts 02543

Dr. J. Ian Collins
Tetra Tech, Inc
630 North Rosemead Boulevard
Pasadena, CA 91107

Dr. L. D. Wright
Coastal Studies Unit
Department of Geography
University of Sydney
Sydney, NSW 2006, Australia

SECURITY CLASSIFICATION OF THIS PAGE *(When Data Entered)*

REPORT DOCUMENTATION PAGE

READ INSTRUCTIONS BEFORE COMPLETING FORM

1. REPORT NUMBER: TR3	2. GOVT ACCESSION NO.: AD-A087 096
3. RECIPIENT'S CATALOG NUMBER:	
4. TITLE *(and Subtitle)*: A Dynamic Process Model for the Beach-Inlet Transition Zone	5. TYPE OF REPORT & PERIOD COVERED: Final Report, Jan. 1, 1977 - June 30, 1980
	6. PERFORMING ORG. REPORT NUMBER:
7. AUTHOR(s): Richard A. Davis, Jr. William T. Fox	8. CONTRACT OR GRANT NUMBER(s): N00014-77-C-0151
9. PERFORMING ORGANIZATION NAME AND ADDRESS: University of South Florida Tampa, Florida 33620	10. PROGRAM ELEMENT, PROJECT, TASK AREA & WORK UNIT NUMBERS: 388-136
11. CONTROLLING OFFICE NAME AND ADDRESS: Geography Programs, Code 462 Office of Naval Research Arlington, VA 22217	12. REPORT DATE: May, 1980 13. NUMBER OF PAGES: 61
14. MONITORING AGENCY NAME & ADDRESS*(if different from Controlling Office)*:	15. SECURITY CLASS. *(of this report)*: Unclassified 15a. DECLASSIFICATION/DOWNGRADING SCHEDULE

16. DISTRIBUTION STATEMENT *(of this Report)*

Unlimited

This document has been approved for public release and sale; its distribution is unlimited.

17. DISTRIBUTION STATEMENT *(of the abstract entered in Block 20, if different from Report)*

18. SUPPLEMENTARY NOTES

19. KEY WORDS *(Continue on reverse side if necessary and identify by block number)*

Beach-inlet transition
Tidal deltas
Longshore currents
Breaker heights
Tidal currents

20. ABSTRACT *(Continue on reverse side if necessary and identify by block number)*

Monitoring of tide and wave generated processes and adjacent to Matanzas Inlet, Florida was conducted during the summer of 1978. Data collected include weather parameters, wave and longshore current measurements, tidal currents and morphology of the inlet and adjacent beach and nearshore area. Measurements were made in a time-series mode in order to provide desired input for anticipated modeling of inlet mouth dynamics.

DD FORM 1 JAN 73 1473 EDITION OF 1 NOV 65 IS OBSOLETE
S/N 0102-LF-014-6601

Unclassified
SECURITY CLASSIFICATION OF THIS PAGE *(When Data Entered)*

Related concurrent projects included drogue studies of tidal currents, sediment transport, bedforms and sediment texture in the inlet.

Weather conditions during the study period were typical of summer conditions on the east coast of Florida. Winds were from the southeast to southwest thereby generating south to north flowing longshore currents. Wind speed was typically less than 10 knots and waves rarely exceeded a meter. Only during the final days of the field study did the wind, wave and longshore current direction shift to a generally north to south direction.

Interactions of tidal inlet processes with open coast processes are significant but restricted to only a few hundred meters of coast adjacent to the inlet. Longshore currents act alternately as a reinforcement and as a hindrance to flow as tides flood and ebb. During flood tides flow on the upcurrent side of the inlet is reinforced and the downcurrent side is hindered. Ebb currents produce the opposite effect on the longshore currents. Beyond the terminal lobe of the ebb tidal delta there is little effect of tidal currents on coastal processes. Here waves are dominant with longshore currents being detectable but masked by waves.

Inlet morphology is an extremely important influence on tidal processes. During flood conditions flow is controlled by channels until shoals are submerged at which time flow is determined primarily by overall inlet shape. Ebbing conditions reflect the reverse situation with channelization of flow during the latter portion of this state. Numerous locations experience ebb and flood directions which change 30 to 40 degrees as the result of combined effects of sand bodies and channels with the overall shape of the inlet.

The simplistic conditions which prevailed during the study period have permitted construction of a dynamic process model for the beach-inlet transitions zone during the tidal cycle. This model depicts the patterns and relative speeds of currents as well as the zones of essentially still water. This model is preliminary and based on only one field study. Further studies and testing of the model are necessary before it can be considered as representative of inlets in general.